

# **Investigating the characterisation, kinetic mechanism, and thermodynamic behaviour of coal-biomass blends in co-pyrolysis process**



**By**

**Hamad Gohar**

**00000318657**

**Session 2019-2021**

**Supervised by**

**Dr. Asif Hussain Khoja**

**U.S. –Pakistan Center for Advanced Studies in Energy (USPCAS-E)**

**National University of Sciences and Technology (NUST)**

**H-12, Islamabad 44000, Pakistan**

**March 2022**

# **Investigating the characterization, kinetic mechanism, and thermodynamic behaviour of coal-biomass blends in co-pyrolysis process**



**By**

**Hamad Gohar**

**00000318657**

**Session 2019-2021**

**Supervised By**

**Dr. Asif Hussain Khoja**

**A Thesis Submitted to U.S. – Pakistan Center for Advanced Studies  
in Energy in partial fulfillment of the requirements for the degree of**

**MASTERS of SCIENCE**

**in**

**THERMAL ENERGY ENGINEERING**

**U.S. – Pakistan Center for Advanced Studies in Energy (USPCAS-E)**

**National University of Sciences and Technology (NUST)**

**H-12, Islamabad 44000, Pakistan**

**March 2022**

## **THESIS ACCEPTANCE CERTIFICATE**

Certified that final copy of MS/MPhil thesis written by Mr. Hamad Gohar, (Registration No. 00000318657), of U.S.-Pakistan Center for Advanced Studies in Energy (USPCASE), NUST has been vetted by undersigned, found complete in all respects as per NUST Statues/Regulations, is in the allowable limits of plagiarism, errors, and mistakes and is accepted as partial fulfillment for the award of MS/MPhil degree. It is further certified that necessary amendments as pointed out by GEC members of the scholar have also been incorporated in the said thesis.

**Signature:** \_\_\_\_\_

**Name of Supervisor:** Dr. Asif Hussain Khoja

**Date:** \_\_\_\_\_

**Signature (HoD TEE):** \_\_\_\_\_

**Date:** \_\_\_\_\_

**Signature (Principal/Dean):** \_\_\_\_\_

**Date:** \_\_\_\_\_

## Certificate

This is to certify that work in this thesis has been carried out by **Mr. Hamad Gohar** and completed under my supervision in Fossil Fuels laboratory, USPCAS-E, National University of Sciences and Technology, H-12, Islamabad, Pakistan.

**Supervisor:**

---

**Dr. Asif Hussain Khoja**  
U.S.-Pakistan Center for Advanced Studies in  
Energy  
NUST, Islamabad

**GEC member 1:**

---

**Dr. Rabia Liaquat**  
U.S.-Pakistan Center for Advanced Studies in  
Energy  
NUST, Islamabad

**GEC member 2:**

---

**Dr. Salman Raza Naqvi**  
SCME  
NUST, Islamabad

**GEC member 3:**

---

**Dr. Abeera Ayaz Ansari**  
U.S.-Pakistan Center for Advanced Studies in  
Energy  
NUST, Islamabad

**HoD-TEE:**

---

**Dr. Majid Ali**  
U.S.-Pakistan Center for Advanced Studies in  
Energy  
NUST, Islamabad

**Principal:**

---

**Prof. Dr. Adeel Waqas**  
U.S.-Pakistan Center for Advanced Studies in  
Energy  
NUST, Islamabad

# Acknowledgments

All praise and thanks to Allah Almighty, who provided me with the power and skills to comprehend, learn, and complete my thesis report.

It gives me great pleasure to express my heartfelt gratitude to my research supervisor, Dr. Asif Hussain Khoja, for allowing me to join the Fossil Fuels Lab study group, USPCAS-E, NUST, Islamabad. I consider myself fortunate to have worked under his supervision. It was a combination of his patience, perseverance, guidance, and inspiration that enabled me to complete my research goals on time. He showed me the approach for conducting research and presenting the findings as clearly as possible.

I owe a debt of gratitude to the members of my GEC committee, Dr. Rabia Liaquat, Dr. Abeera Ayaz Ansari, and Dr. Salman Raza Naqvi who honored my committee's presence. I'd want to express my gratitude to my colleagues and friends for their unwavering support. I'd want to express my gratitude to Lab Engineers Mr. Ali Abdullah for his unwavering assistance throughout the research.

I owe my parents and my siblings a debt of gratitude for their love, prayers, care, and sacrifices in educating and preparing me for the future.

# Abstract

Co-pyrolysis of the coal-biomass blend has wide-ranging application prospects in relieving energy crises and environmental pollution. In this study, coal-biomass (hemp, sawdust) blends were prepared at various blending ratios (20-80%) for co-pyrolysis investigating. The coal-biomass blends were characterized using ultimate analysis (CHN), gross calorific value (GCV), Fourier transform infrared spectroscopy (FTIR). The co-pyrolysis of blends was performed in thermogravimetric analyzer (TGA). Furthermore, the synergistic effect in each blend was observed by the deviation between the experimental and calculated data of mass loss (ML), residue left (RL), and maximum mass loss rate ( $DTG_{max}$ ). The values of deviation in ML and  $DTG_{max}$  indicated the synergistic effect and inhibitory effect during co-pyrolysis. Kinetic parameters were analyzed by employing the Coats-Redfern method with thirteen integral functions. The activation energy ( $E_a$ ) for individual coal (100C) was 39 kJ/mol through one and half chemical reaction (F3/2), while individual sawdust (100SD) and hemp (100H) showed 60 kJ/mol through deceleratory reaction mechanism for contracting sphere (R3) and 44 kJ/mol through the second order chemical reaction (F2), respectively. Thermodynamic parameters such as change in enthalpy ( $\Delta H$ ), change in Gibbs free energy ( $\Delta G$ ) showed positive values, while the change in entropy ( $\Delta S$ ) was negative for each coal-biomass blend. The C-SD blends are suitable to produce bio-oil as 100SD contained a larger number of volatiles, whereas the C-H blends are suitable to produce bio-char as 100H produced more residue after co-pyrolysis. Hemp bio-char was further characterized by FTIR, TGA, and SEM-EDX analysis to investigate its potential in environmental and energy applications.

**Keywords:** *Hemp pyrolysis, coal-biomass blends, Co-pyrolysis, Synergistic effects, Kinetics & Thermodynamics, Bio-char*

# Table of Contents

<b>Abstract.....</b>	<b>I</b>
<b>List of Figures.....</b>	<b>V</b>
<b>List of Tables .....</b>	<b>VI</b>
<b>List of Publications.....</b>	<b>VII</b>
<b>List of Abbreviations .....</b>	<b>VIII</b>
<b>Chapter 1 Introduction.....</b>	<b>1</b>
<b>1.1 Background .....</b>	<b>1</b>
<b>1.2 Problem statement .....</b>	<b>3</b>
<b>1.3 Research hypothesis .....</b>	<b>3</b>
<b>1.4 Objectives of study.....</b>	<b>4</b>
<b>1.5 Scope of study.....</b>	<b>5</b>
<b>1.6 Flow chart of thesis.....</b>	<b>6</b>
<b>Summary .....</b>	<b>8</b>
<b>References.....</b>	<b>9</b>
<b>Chapter 2 Literature Review .....</b>	<b>11</b>
<b>2.1 Coal Overview.....</b>	<b>11</b>
<b>2.2 Biomass Overview and utilization.....</b>	<b>13</b>
<b>2.3 Co-pyrolysis.....</b>	<b>18</b>
<b>2.3.1 Synergistic effect.....</b>	<b>20</b>

<b>2.4 Co-pyrolysis parameters and synergistic effect .....</b>	<b>20</b>
2.4.1 Feedstock type.....	20
2.4.2 Blending ratio.....	21
2.4.3 Heating rate .....	23
2.4.4 Operating temperature.....	23
2.4.5 The reactor types .....	24
<b>2.5 Thermo-Kinetics Analysis.....</b>	<b>25</b>
2.5.1 Kinetic modeling overview .....	25
2.5.2 Model fitting and model free overview.....	26
2.5.3 Thermodynamics parameters .....	29
<b>Summary .....</b>	<b>31</b>
<b>References.....</b>	<b>32</b>
<b>Chapter 3 Material and Method .....</b>	<b>40</b>
<b>3.1 Sample collection and blends preparation .....</b>	<b>40</b>
<b>3.2 Samples characterization .....</b>	<b>41</b>
<b>3.3 Synergistic effect .....</b>	<b>42</b>
<b>3.4 Kinetics study .....</b>	<b>42</b>
<b>3.5 Thermodynamics parameters.....</b>	<b>45</b>
<b>3.6 Experimental setup for the bio-char formation.....</b>	<b>46</b>
3.6.1 Bio-char characterization .....	47
<b>Summary .....</b>	<b>48</b>

References.....	49
<b>Chapter 4 Results and Discussion.....</b>	<b>50</b>
<b>4.1 Materials Characterization.....</b>	<b>50</b>
4.2 Synergistic effect .....	60
4.3 Kinetics Study .....	62
4.4 Thermodynamics parameters.....	65
4.5 Bio-char characterization .....	67
Summary .....	71
References.....	73
<b>Chapter 5 Conclusions and Recommendations.....</b>	<b>76</b>
5.1 Conclusions.....	76
5.2 Recommendations.....	77
<b>Appendix A .....</b>	<b>78</b>

# List of Figures

Figure 1-1 CO <sub>2</sub> intake and emission cycle for conventional and renewable fuels.....	2
Figure 1-2 Steps involved in the research scope.....	6
Figure 1-3 Thesis flow diagram .....	7
Figure 2-1 Coal classification, availability, and utilization around the world .....	12
Figure 2-2 Biomass utilization pathway for renewable fuels production .....	15
Figure 2-3 Biomass pyrolysis in a fixed bed reactor for the making of valuable products .....	17
Figure 2-4 Residue mass vs the temperature for coal-biomass blends [69].....	22
Figure 3-1 Coal-biomass samples and blends preparation schematic diagram.....	40
Figure 3-2 Hemp bio-char production via fixed bed reactor schematic diagram .....	47
Figure 4-1 GCV measurement of coal-biomass blends (a) C-SD (b) C-H .....	52
Figure 4-2 FTIR analysis of coal-biomass blends (a) C-SD (b) C-H .....	54
Figure 4-3 TGA/DTG of coal-biomass blends (a) C-SD TGA (b) C-SD DTG (c) C-H TGA (d) C-H DTG.....	58
Figure 4-4 E <sub>a</sub> of thirteen models for coal-biomass samples (a) C-SD first stage (b) C-SD second stage (c) C-H first stage (d) C-H second stage .....	64
Figure 4-5 Characterisation of raw hemp and hemp-derived bio-char (a) FTIR (b) TGA .....	68
Figure 4-6 Hemp-derived bio-char (a-c) SEM analysis (d) EDX elemental analysis.....	70

# List of Tables

Table 2-1 The production of H <sub>2</sub> and syngas through biomass thermochemical processes .....	16
Table 2-2 Literature on coal-biomass studies .....	19
Table 2-3 Comprehensively used model fitting and model free methods, general forms, and assumption [109] .....	28
Table 3-1 Algebraic expressions for reaction mechanism $g(\alpha)$ for solid state reaction .....	44
Table 4-1 Ultimate analysis (CHN) of coal-biomass blends .....	51
Table 4-2 Major portions of decomposition of coal-biomass and their blends during pyrolysis in N <sub>2</sub> environment.....	59
Table 4-3 Synergistic effect calculation in co-pyrolysis of coal-biomass blends.....	61
Table 4-4 Co-pyrolysis kinetics parameters calculation for coal-biomass blends.....	65
Table 4-5 Co-pyrolysis thermodynamic parameters calculation for coal-biomass blends .....	66

# List of Publications

1. “Investigating the characterisation, kinetic mechanism, and thermodynamic behaviour of coal-biomass blends in co-pyrolysis process”. Hamad Gohar<sup>1</sup>, Asif Hussain Khoja\*, Abeera Ayaz Ansari, Rabia Liaquat, Salman Raza Naqvi, Muhammad Hassan, Khalil Hasni, Umair Yaqub Qazi and Imtiaz Ali. Process Safety and Environmental Protection. (**Under review**)

# List of Abbreviations

<b>Abbreviation:</b>	<b>Description:</b>
<b>A</b>	Pre-exponential factor
<b>C-H</b>	Coal-hemp
<b>C-SD</b>	Coal-sawdust
<b>DTG</b>	Derivative thermogravimetry
<b>E<sub>a</sub></b>	Activation energy
<b>EDX</b>	Energy Dispersive X-Ray Analysis
<b>FBR</b>	Fixed bed reactor
<b>FTIR</b>	Fourier transform infrared spectroscopy
<b>GCV</b>	Gross calorific value
<b>GHG</b>	Greenhouse gasses
<b>IEA</b>	International Energy Agency
<b>K</b>	Rate constant
<b>ML</b>	Mass loss
<b>R</b>	Gas constant
<b>R<sup>2</sup></b>	Linear regression

<b>RL</b>	Residue left
<b>SEM</b>	Scanning electron microscope
<b>TGA</b>	Thermal gravimetric analysis
<b>DTG<sub>max</sub></b>	Maximum weight loss rate
<b>f(<math>\alpha</math>)</b>	Reaction model
<b>g(<math>\alpha</math>)</b>	Integral function
<b>T<sub>i</sub></b>	Ignition temperature
<b>T<sub>p</sub></b>	Peak decomposition temperature
<b><math>\alpha</math></b>	Conversion factor
<b>B</b>	Heating rate
<b><math>\Delta G</math></b>	Change in Gibbes free energy
<b><math>\Delta H</math></b>	Change in enthalpy
<b><math>\Delta S</math></b>	Change in entropy

# Chapter 1

## Introduction

### 1.1 Background

In a developed country, the energy production by reliance on fossil fuels (Coal, Natural Gas, and conventional oil) is the keystone for economic growth. However, the penalty should be paid with accelerated economic growth [1] in terms of reserves depletion which will further increase the cost of fossil fuels in upcoming years. Alongside, the consumption of fossil fuels is causing destructive emissions (like CO<sub>2</sub>, SO<sub>x</sub>, and NO<sub>x</sub>) for living things on the planet that ultimately destroy the ecosystem [2]. At present, the gas and oil sectors are under challenges about how to produce sustainable energy from conventional resources to partially save their reserves. Natural gas and oil are considered as the rapidly depleting source of energy in the future, but coal reserves can show a significant contribution to encounter a global energy demand in the future because coal reserves will be available up to the next two hundred years. While natural gas sixty-five and oil will be available up to forty years [3].

Therefore, coal remains the prominent source of energy for power generation and domestic uses across the globe [4]. More coal is being used with industrial development and increased energy demand. There is two main consideration that should be kept in mind when utilizing coal, the first one is the harmful emissions which emits after its combustion like CO<sub>2</sub>, NO<sub>x</sub>, and SO<sub>x</sub> [4, 5]. And the second one is the reserves that will deplete faster rate than right now because all the energy productions will mainly rely on coal. As a result, finding renewable and ecologically favourable feedstock for a long-term supply of fuels and energy is essential [6].

However, to reduce the emissions, sustainable utilization of coal is under development and global research with strong importance on CO<sub>2</sub> reduction and inexpensive energy supply. The vast coal deposits may be exploited to make synthetic oil

and other valuable products such as char, syngas, and other materials that can be used to partially replace consumption of conventional oil and gas. Additionally, pyrolysis of coal is a suitable option to produce liquid and solid fuels that are low sulfur and phosphor content as well as low ash content [7]. Among renewables supply for partial substitute of coal reserves, biomass gained more interest due to its wide abundance and CO<sub>2</sub> neutrality in the atmosphere during utilization as compared to fossil fuels [8] as shown in Figure 1-1. More than half of global research over the last three decades has focused on biomass energy source [9]. Biomass can be transformed to biofuels and biochemical products through several methods [5].

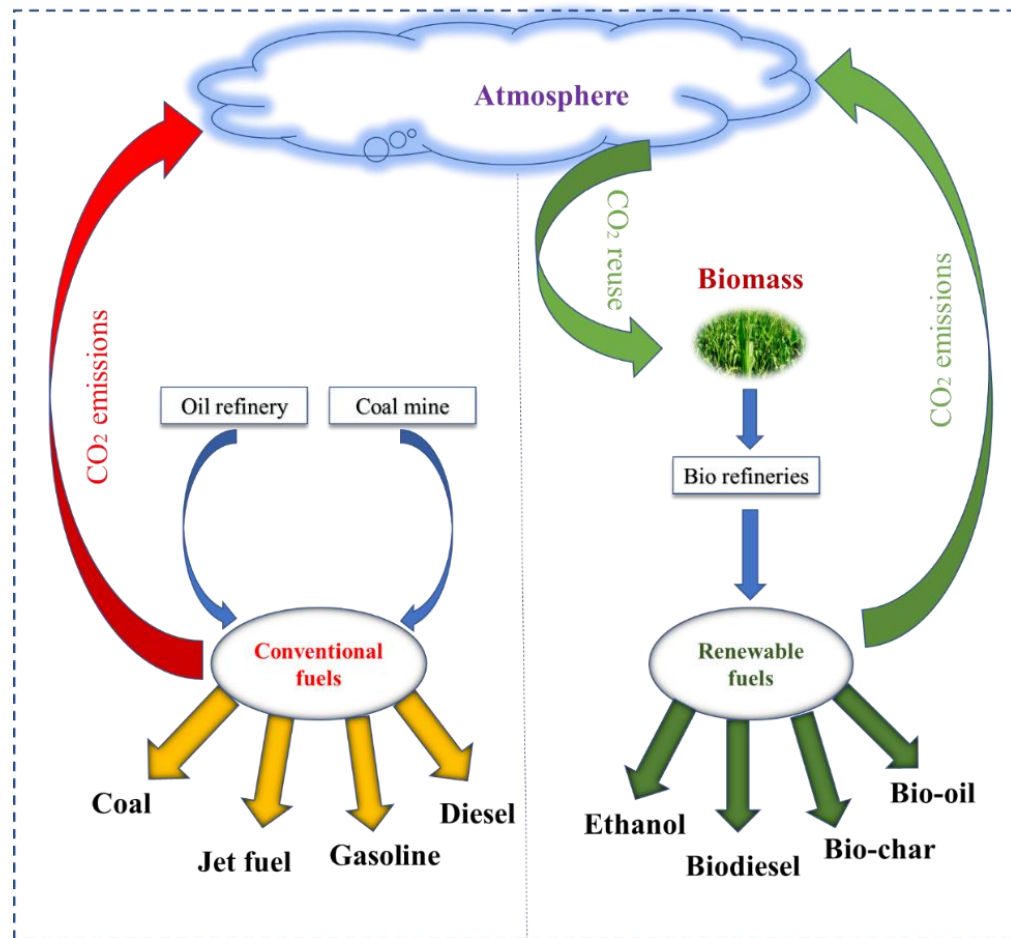


**Figure 1-1** CO<sub>2</sub> intake and emission cycle for conventional and renewable fuels (self-created)

Biomass pyrolysis has recently attracted increasing attention among these approaches because it may create three useful products: bio-oil, bio-char, and biogas [10, 11]. Pyrolysis oil utilized as a fuel or a feedstock for a variety of commercial chemicals. Boilers, and turbines may all use bio-oil directly [12]. Furthermore, pyrolysis oil has received excellent reviews due to its less emissions.[12, 13].

## **1.2 Problem statement**

The yield and quality of coal pyrolysis products to form synthetic fuels are relatively poor due to the low hydrogen-to-carbon ratio of coal [14]. Furthermore, large-scale biomass operations for the production of biofuels and value-added goods would need the use of biomass mixes rather than a single kind of biomass, necessitating the use of biomass blends rather than a single type of biomass. [15]. Therefore, it is a challenge to explore and characterize more types of biomass to reduce the problem with the seasonal availability of biomass [16]. Despite being environmentally beneficial, pyrolysis oil has inferior fuel qualities than fossil fuels, notably in terms of ignition proficiency. This difficulty is caused by the high proportion of oxygenated chemicals in pyrolysis oil in this scenario [11, 17, 18]. Furthermore, the high moisture and oxygen content of pyrolysis oil causes corrosion, low caloric value, and instability [12, 19].

It is difficult to find out optimum blending ratio for the coal-biomass blend to gain a more synergistic effect during coal-biomass co-pyrolysis. Furthermore, the thermo-kinetics of coal and biomass is a crucial parameter that needs to be evaluated for designing and scaling of pyrolysis reactor [20]. The kinetics evaluation of coal and biomass is a complex process because many chemical reactions may involve during its thermal degradation [21]. As a result, understanding kinetic and thermodynamic characteristics is critical for building a pyrolysis process that is both efficient and long-lasting [22].

## **1.3 Research hypothesis**

The combination of coal with biomass could be utilized to counter seasonality of biomass and provide a long-term feedstock [23]. The utilization of biomass for co-

pyrolysis with coal can accelerate the cracking of coal, resulting in higher-quality and yielding products than individual coal pyrolysis. The biomass contains more hydrogen, making it a hydrogen donor during co-pyrolysis to increase coal cracking [24]. Furthermore, combining coal with biomass is a potential option for reducing unsustainable fossil fuel consumption as well as pollution concerns. [25]. Co-pyrolysis is also beneficial to biomass since it increases the calorific value of products and reduces process instability caused by highly oxygenated molecules in bio-oil. For this purpose, Coal-Sawdust (C-SD) and Coal-Hemp (C-H) blends were prepared at various blending ratios and characterized to evaluate the physical and chemical properties of coal-biomass blends. Each blending ratio was characterized to find out the optimum blending ratio to gain a more synergistic effect. Additionally, the kinetics and thermodynamic parameters of C-SD and C-H blends were calculated through a detailed study to evaluate the reaction mechanism for each stage of decomposition which will help in designing and scaling of co-pyrolysis reactor.

#### **1.4 Objectives of study**

The research conducted in this thesis mainly focuses on the co-pyrolysis of coal-biomass blends. The goal of this study is to develop and investigate the characterization of coal-biomass blends in order to assess the chemical and physical properties of separate coal and biomass, as well as how these qualities may change when coal and biomass are blended. The experimental work reported in this study is consistent and agrees with previous studies. The study's key objectives are as follows:

- To prepare coal-biomass blends and evaluate their characteristics at various blending ratios.
- To find out the optimum blend having the highest synergistic effects.
- To find out the kinetics and thermodynamic parameters through the Coats-Redfern method that will help in approaching the most suitable reaction mechanism for each stage of decomposition during pyrolysis and co-pyrolysis.

- To prepare and investigate the characterization of hemp bio-char for the seek of its suitable applicability.

## 1.5 Scope of study

For modelling of the co-pyrolysis system, coal-biomass blends were prepared and characterized. After gathering the materials, the bituminous coal (100C), sawdust (100SD), and wild hemp (100H) were dried in an oven for 24 hours at 105 °C to remove moisture. After screening, both coal and biomass had particle sizes of 0.63 mm. Several factors influence coal and biomass co-pyrolysis, including feedstock type, blending ratio, heating rate, reaction mechanism, and reactor design. The scope of the research is shown in Figure 1-2. For the co-pyrolysis process, several blending ratios of coal-biomass blends were generated in this investigation. Ultimate analysis (CHN), gross calorific value (GCV), and Fourier transform infrared spectroscopy were used to analyses the coal-biomass blends (FTIR). TGA analysis of coal-biomass samples was also carried out in an inert (N<sub>2</sub>) atmosphere to assess their co-pyrolysis behavior. The synergistic effects were calculated using the difference between experimental and computational data. The Coat-Redfern approach was used to compute kinetics parameters such as activation energy (E<sub>a</sub>) and pre-exponential factor (A) using thirteen integral functions. Changes in enthalpy (H), Gibbs free energy (G), and entropy (S) were calculated as well as other thermodynamic parameters. The 100H is pyrolyzed to form bio-char, and hemp-derived bio-char is further processed.

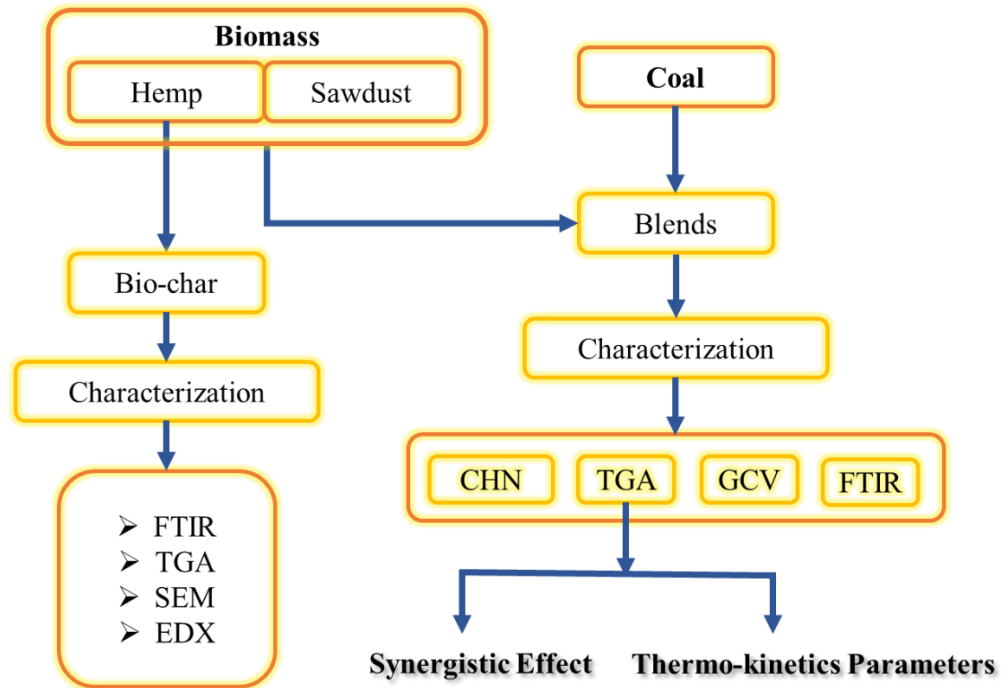


**Figure 1-2** Steps involved in the research scope (self-created).

## 1.6 Flow chart of thesis

The thesis flow chart is presented in Figure 1-3. The goal of the study was to see how biomass and coal could be used more efficiently and sustainably instead of being wasted in landfills or causing damaging pollutants. A literature review was undertaken on both coal and biomass current statistics and utilisation for this purpose. CHN, GCV, FTIR, and TGA were used to prepare and characterize coal-biomass blends. The TGA data was also used to describe the co-pyrolysis process in terms of kinetics and thermodynamics. The hemp bio-char was made in a fixed bed reactor and then characterized using FTIR, TGA, and SEM-EDX to determine its suitability for use in the energy and agriculture fields. In the results and discussion section, the data from the results were carefully reviewed.

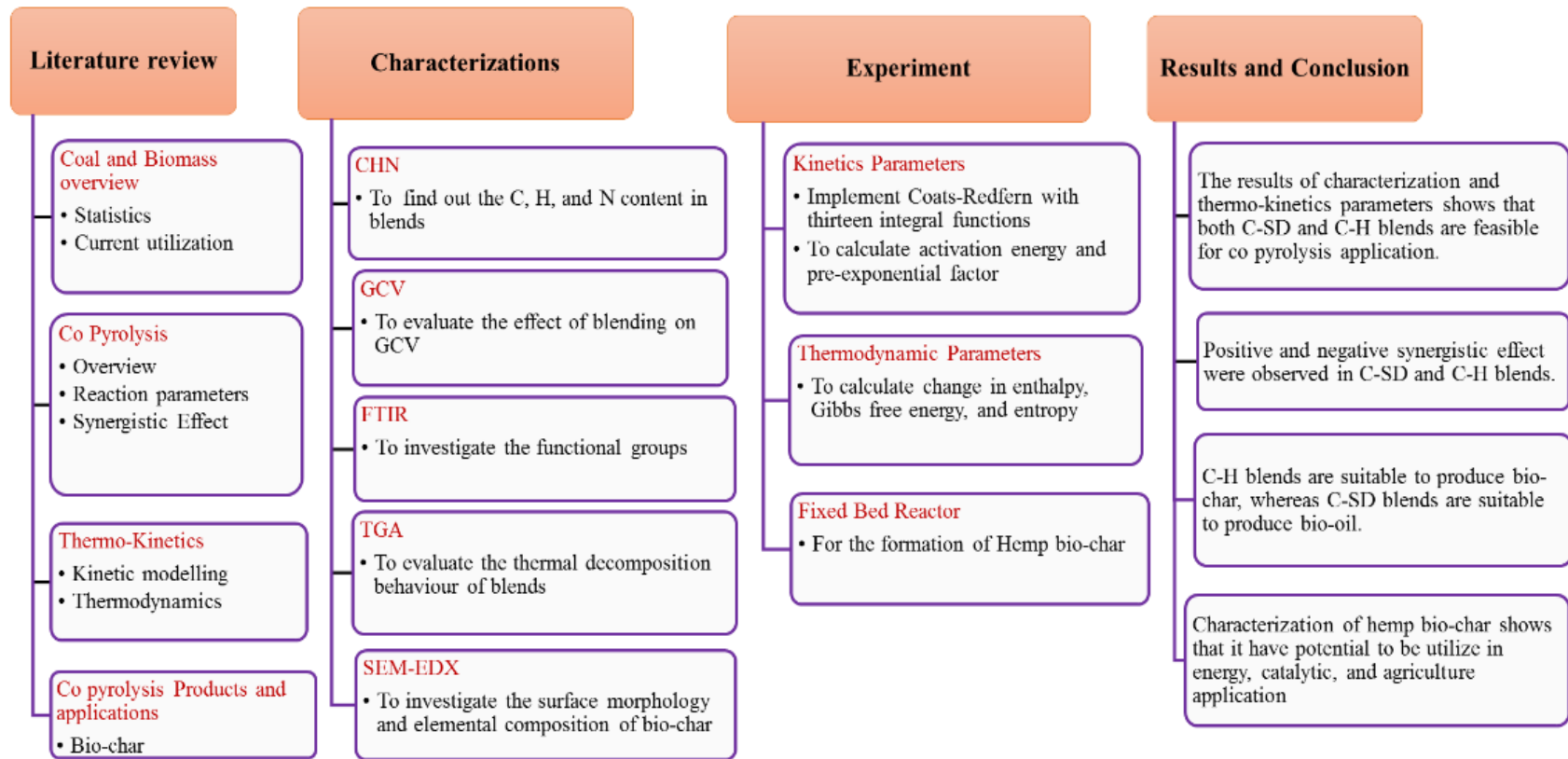


**Figure 1-3** Thesis flow diagram (self-created)

## Summary

As the energy demand is increasing with the industrialization. There are number of fossil fuel (coal, natural gas, natural oil) that play a prominent role in fulfilling the energy demand. However, fossil fuels are depleting and causes serious environmental damage. According to the literature, coal will be available for up to 200 years, whereas natural gas (65 years) and natural oil would be available for only 65 years (40 years). Therefore, it is need of time to partially or completely substitute fossil fuels with sustainable fuels. Biomass is one of the potential fuel sources in all over the world. But there is some problem in biomass utilization such as in pyrolysis the high moisture, oxygen content causes the low calorific value of fuel. Also, excessive amount of these content causes fouling and slagging in boiler. As a result, this study looked at the co-pyrolysis of coal-biomass blends. Co-pyrolysis solves the challenges associated with individual coal and biomass pyrolysis. Furthermore, combining biomass and coal reduces harmful emissions because biomass is carbon neutral and contains less Sulphur and nitrogen.

## References

1. REN, R.J.R.e.p.n.f.t.s.c.P., France: REN21 Secretariat, *Global status report*. 2015.
2. Vuthaluru, H.B., *Thermal behaviour of coal/biomass blends during co-pyrolysis*. Fuel Processing Technology, 2004. **85**(2): p. 141-155.
3. Ismail, T.M., et al., *Coal and biomass co-pyrolysis in a fluidized-bed reactor: Numerical assessment of fuel type and blending conditions*. Fuel, 2020. **275**: p. 118004.
4. Mushtaq, F., R. Mat, and F.N. Ani, *A review on microwave assisted pyrolysis of coal and biomass for fuel production*. Renewable and Sustainable Energy Reviews, 2014. **39**: p. 555-574.
5. Merdun, H., Z.B. Laougé, and A.S. Çiğgin, *Synergistic effects on co-pyrolysis and co-combustion of sludge and coal investigated by thermogravimetric analysis*. Journal of Thermal Analysis and Calorimetry, 2021.
6. Hu, X. and M. Gholizadeh, *Biomass pyrolysis: A review of the process development and challenges from initial researches up to the commercialisation stage*. Journal of Energy Chemistry, 2019. **39**: p. 109-143.
7. Huang, Y., et al., *Co-pyrolysis of bituminous coal and biomass in a pressured fluidized bed*. Chinese Journal of Chemical Engineering, 2019. **27**(7): p. 1666-1673.
8. Anand, V., V. Sunjeev, and R. Vinu, *Catalytic fast pyrolysis of *Arthrospira platensis* (spirulina) algae using zeolites*. Journal of Analytical and Applied Pyrolysis, 2016. **118**: p. 298-307.
9. Manzano-Agugliaro, F., et al., *Scientific production of renewable energies worldwide: An overview*. Renewable and Sustainable Energy Reviews, 2013. **18**: p. 134-143.
10. Bridgwater, T., *Biomass for energy*. Journal of the Science of Food and Agriculture, 2006. **86**(12): p. 1755-1768.
11. Guillain, M., et al., *Attrition-free pyrolysis to produce bio-oil and char*. Bioresource Technology, 2009. **100**(23): p. 6069-6075.
12. Abnisa, F. and W.M.A. Wan Daud, *A review on co-pyrolysis of biomass: An optional technique to obtain a high-grade pyrolysis oil*. Energy Conversion and Management, 2014. **87**: p. 71-85.
13. Vitolo, S., et al., *Catalytic upgrading of pyrolytic oils to fuel over different zeolites*. Fuel, 1999. **78**(10): p. 1147-1159.
14. Miura, K., *Mild conversion of coal for producing valuable chemicals*. Fuel Processing Technology, 2000. **62**(2): p. 119-135.
15. Defoort, F., et al., *Physicochemical Approach To Blend Biomass*. Energy & Fuels, 2019. **33**(7): p. 5820-5828.
16. Jin, X., et al., *Co-pyrolysis of rice straw and water hyacinth: Characterization of products, yields and biomass interaction effect*. Biomass and Bioenergy, 2019. **127**: p. 105281.
17. Oasmaa, A. and S. Czernik, *Fuel Oil Quality of Biomass Pyrolysis Oils State of the Art for the End Users*. Energy & Fuels, 1999. **13**(4): p. 914-921.
18. Parihar, M.F., et al., *An Experimental Study on Pyrolysis of Biomass*. Process

- Safety and Environmental Protection, 2007. **85**(5): p. 458-465.
19. Lu, Q., W.-Z. Li, and X.-F. Zhu, *Overview of fuel properties of biomass fast pyrolysis oils*. Energy Conversion and Management, 2009. **50**(5): p. 1376-1383.
  20. White, J.E., W.J. Catallo, and B.L. Legendre, *Biomass pyrolysis kinetics: A comparative critical review with relevant agricultural residue case studies*. Journal of Analytical and Applied Pyrolysis, 2011. **91**(1): p. 1-33.
  21. Gouws, S.M., et al., *Co-pyrolysis of coal and raw/torrefied biomass: A review on chemistry, kinetics and implementation*. Renewable and Sustainable Energy Reviews, 2021. **135**: p. 110189.
  22. Merdun, H. and Z.B. Laougé, *Kinetic and thermodynamic analyses during co-pyrolysis of greenhouse wastes and coal by TGA*. Renewable Energy, 2021. **163**: p. 453-464.
  23. Li, S., et al., *Study on co-pyrolysis characteristics of rice straw and Shenfu bituminous coal blends in a fixed bed reactor*. Bioresource Technology, 2014. **155**: p. 252-257.
  24. Hassan, H., J.K. Lim, and B.H. Hameed, *Recent progress on biomass co-pyrolysis conversion into high-quality bio-oil*. Bioresource Technology, 2016. **221**: p. 645-655.
  25. Meng, H., et al., *Study on product distributions and char morphology during rapid co-pyrolysis of platanus wood and lignite in a drop tube fixed-bed reactor*. Bioresource Technology, 2016. **209**: p. 273-281.

# Chapter 2

## Literature Review

### 2.1 Coal Overview

Carbon and hydrocarbons, which have a high energy density and are produced when coal is burned, make up the majority of coal (burning). During the First Industrial Revolution, coal-burning became a movement. From an economic aspect, this energy source was revolutionary. On the other hand, ambient air pollution is harmful to the environment. [1-3]. Coal production is continuing to rise due to increased demand for low-cost energy, iron and steel, and cement. With an estimated 1.1 trillion tonnes of confirmed coal reserves worldwide, coal will last around 115 years longer than conventional oil and gas reserves, depending on current extraction rates. The production of coal in the world is dominated by ten countries, which account for 90% of total output. For the past three decades, China has been the world's greatest coal producer (with almost a third of the world's total reserves), followed by the United States of America, India, Australia, Indonesia, Russia, South Africa, Kazakhstan, Columbia, and Ukraine [4].

Coal is the second most important energy source on the planet, accounting for 40% of worldwide primary energy use.[5]. In major developing nations, coal is utilized as an primary energy source. In December 2015, all nations committed in Paris to invest and intensify efforts to prevent global warming to achieve a sustainable, low-carbon future. The Paris Agreement aims to lower greenhouse gas emissions [6]. Most poor countries are more preoccupied with the here and now than with the future, hence the goals are unlikely to be met. Power plants release toxins into the environment, which can harm people's health [7]. Not only the burning of coal is a health risk but the huge amount of coal dust produced during extractions, transportation is also a cause of xenobiotic diseases for workers and nearby neighborhoods [8].

Low and middle income nations with around 97% of their cities having population higher than 0.1 million do not fulfill WHO air quality recommendations [9]. Although coal combustion is one of the contaminants, it is also crucial to highlight that coal transportation, point-source household heating, cooking sources, and automobile fuel combustion all contribute to environmental pollution. An organism's ability to operate properly is dependent on the quality of the air it breathes [10]. Figure 2-1 illustrates the classification, availability, and the path for each type effect utilization of coal:

Lignite (60-75 percent carbon on a dry ash-free basis, 30-70 percent moisture): Lignite is completed from compacted peat. It is also a low-rank coal which is very volatile and majorly utilized in power plants. It is employed in the generation of power. Polished "jet" lignite is often used to make ornamental stones [11].

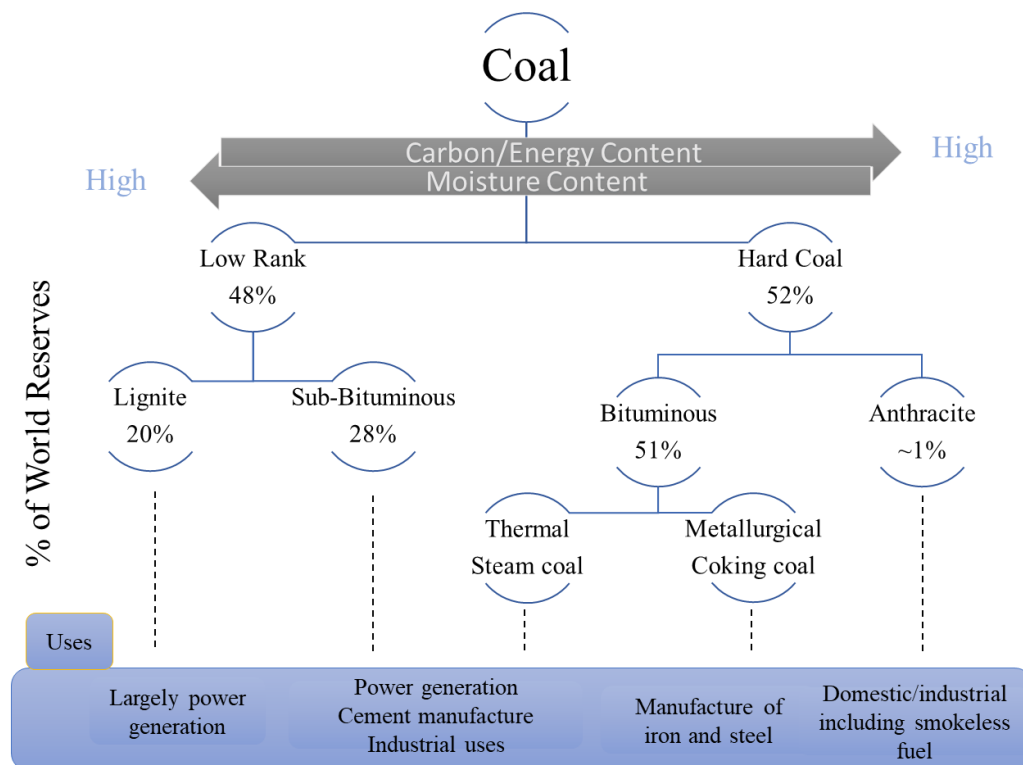


**Figure 2-1** Coal classification, availability, and utilization around the world (self-created)

Sub-bituminous Coal: (carbon content ranges from 71 to 77 percent on a dry ash-free basis): It's substantial and ranges from dusky brown to lean black having 15-30% moisture content. This sort of coal has a heat content ranging from 8300 to 11500 BTU/lb. It's used to generate steam-powered electricity [12].

Bituminous coal (carbon content ranging from 77 to 87 percent): This type of coal is dense black having 77-87% carbon content along with a moisture level of 1.5-7 percent. Bituminous coal is dense, black coal made from compressed broken down lignite. These coals are commonly used in the production of briquettes and power plants, as well as the production of coke. When compared to lignite coal, it has two to three times the heat content [13].

Anthracite (carbon content ranges from 86 to 97 percent): It's the best ignitable coal, with a black vitreous sheen. It is the most abrasive type of coal. It is a non-smoking fuel that is mostly used in residential and commercial settings. It produces a lot of heat and burns for a long period. It has a relatively low Sulphur concentration [14]. In Pakistan, coal accounts for only 0.2 percent of total electricity output. It is mostly used to generate heat. It is cost-effective but harmful to the environment. If the correct coal policies are implemented, it can result in a sharp increase. Pyrolysis of coal forms liquids and other compounds, however because of the low amount of hydrogen, the yield is low [15]. Coal pyrolysis is an exciting technology for improving fluid quality and production, but expensive hydrogen prevents it from being widely used in business [16].

## **2.2 Biomass Overview and utilization**

One of the potential abundant energy resources globally, are biomass resources; annual primary output exceeds 4500 EJ, having 2900 EJ as potential bioenergy, about 270 EJ of which is sustainable. Currently, global biomass residues and wastes, which include by-products of food, fiber, and forest production, exceeded 110 EJ per year, with only approximately 10% of that being exploited for energy. In the commercial sector, residues concentrated at industrial sites are currently the most extensively used biomass source [17]. Each year, Pakistan produces approximately 220 billion tonnes of biomass and

municipal solid waste, indicating a considerable improvement in energy production. A considerable percentage of it is burned inefficiently in open areas, polluting the environment. The IEA (International Energy Agency) suggested that biofuels might meet roughly 27% of the world's fuel demands through 2050. This suggests that biofuels have a lot of potential and are a viable answer for the masses' future energy demands. Agricultural waste is employed as biomass fuel for renewable energy generation in advanced countries, while biomass is still underutilized in developing countries. The world bank has released an atlas that includes a report on Pakistan's biomass energy potential, which includes locations such as sugar mills, rice plants, municipal solid waste dumps, and dairy farms. Crop leftovers left in agricultural fields which are left or thrown away because they are of no use.

Crop processing leftovers have a potential of 25.3 million tonnes per year, with an equal energy potential of 61,838 GWh/year, while crop harvesting residues have a potential of 114 million tonnes per year, with an equivalent energy potential of 448,990 GWh/year, according to the report. Pakistan is expected to collect about 20 million tonnes of organic waste, up 2.4 percent from last year. Every day, Karachi produces roughly 9000 tonnes of municipal waste. When energy-saving measures are performed, on the one hand, reliance on conventional fossil fuels can be minimized and eventually phased out if significant consideration is given to biomass fuel technology adaption on a wider scale [18]. Hemicellulose, lignin, and cellulose are the three main components that make up the majority of biomass. Hemicellulose is a polysaccharide made up of smaller chains (500-3000 sugar units) that accounts for 25-30% of biomass. At 150 degrees Celsius, hemicellulose begins to disintegrate, and at 200 degrees Celsius, significant weight loss occurs. During the thermal decomposition of hemicellulose, light volatiles are released, resulting in less char and tars [19]. The fibrous part of wood and biomass is cellulose, a polymer with a molecular weight of 106 and higher. Because cellulose has a more crystalline structure than hemicellulose, it resists heat breakdown. At temperatures between 240 and 350 degrees Celsius, cellulose decomposes [20]. Lignin is a plant cell wall component that fills in the gaps between cellulose, hemicellulose, and pectin components. The thermal breakdown of lignin begins at temperatures between 280 and

500 degrees Celsius, creating phenols [21]. Biochemical and thermochemical processes can convert biomass into fuels and chemicals, as shown in Figure 2-2. The Pyrolysis, hydrothermal liquefaction, gasification, combustion, and hydrothermal carbonization are the most common thermochemical processes [22]. Table 2-1 presented the yield of products generated by thermochemical conversion of biomass. Biomass pyrolysis performed in a different type of reactor and reactor type affects the yield of product that is presented in the below section.

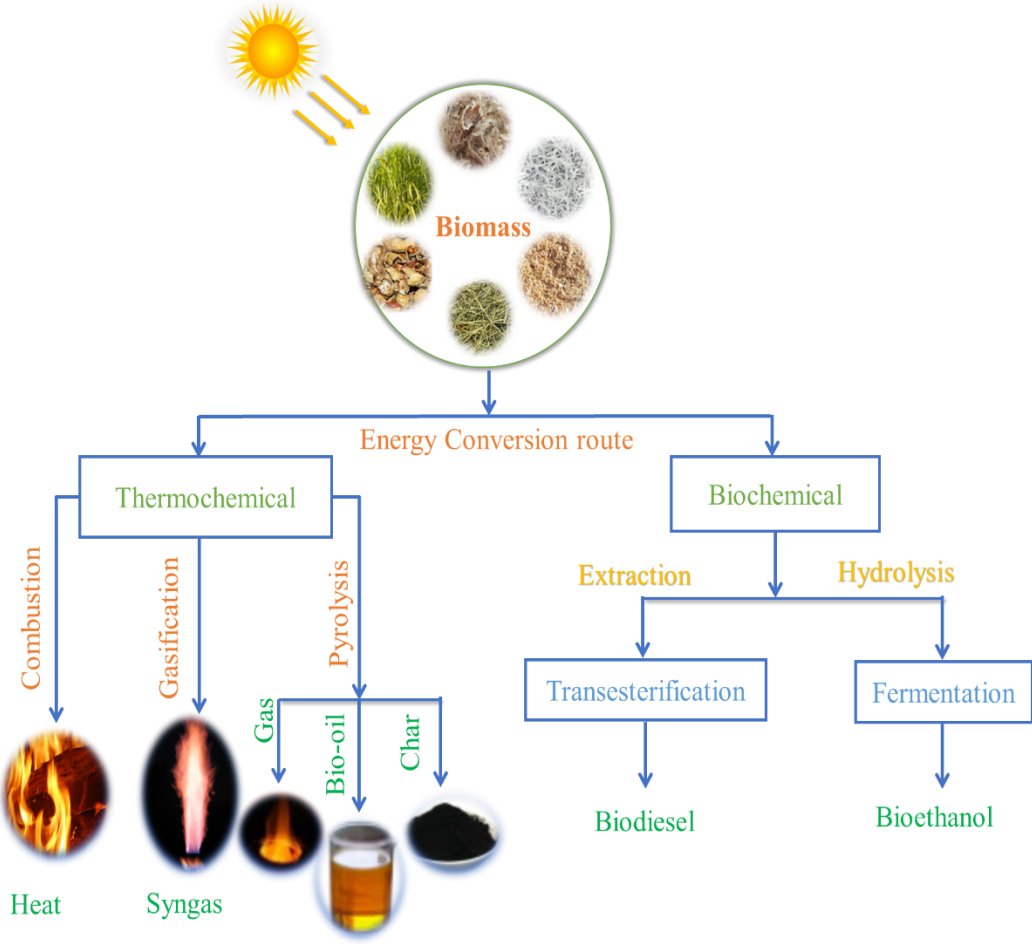


**Figure 2-2** Biomass utilization pathway for renewable fuels production (self-created)

Biomass pyrolysis is a thermochemical process that happens when there is a restricted or no supply of oxygen, preventing excessive gasification. To generate a high yield of hydrogen-enriched syngas, this process is often run at a high temperature (600–900°C), with modest heating rates and a lengthy residence time.

In biomass pyrolysis, fast pyrolysis uses rapid heating rates and short hot vapor residence periods (less than one second) to produce a liquid with a 75% yield. The pyrolysis liquid, also known as bio-oil, has the potential to be developed into transportation fuels and high-value chemicals. To generate the energy required for the pyrolysis reaction, char and some gaseous products such as methane could be combusted. The technology of biomass pyrolysis is gaining prominence in academia and business due to the rising need for liquid transportation fuels [22, 23]. Pyrolysis can be done using atmospheric pressure. As a result, pyrolysis has aroused people's interest in turning biomass to a liquid fuel. Biomass pyrolysis is separated into two forms based on the heating rate: slow and quick pyrolysis. Fast pyrolysis is presently the preferred approach because to its rapid reaction rate and significantly higher bio-oil yields [24].

**Table 2-1** The production of H<sub>2</sub> and syngas through biomass thermochemical processes

<b>Feedstock</b>	<b>H<sub>2</sub> (vol%)</b>	<b>Syngas (vol%)</b>	<b>Ref.</b>
Rice husk	41.20	67.86	[25]
Sawdust pellets	20.43	43.03	[26]
Municipal solid waste and wheat straw	-	47-48	[27]
Corn stalk bale	~35	>50	[28]

Fast pyrolysis has been the subject of a variety of studies, including the study of pyrolysis mechanisms, reaction processes, and reactor design, as well as the creation of catalysts for catalytic pyrolysis. During pyrolysis, many writers investigated the reaction routes of biomass components. Figure 2-3 illustrates the conversion of biomass and their obtained products through a fixed bed reactor. For biomass pyrolysis, three key mechanisms are considered: char production, depolymerization, and fragmentation. Cracking and recombination are examples of secondary reactions that can occur [24].

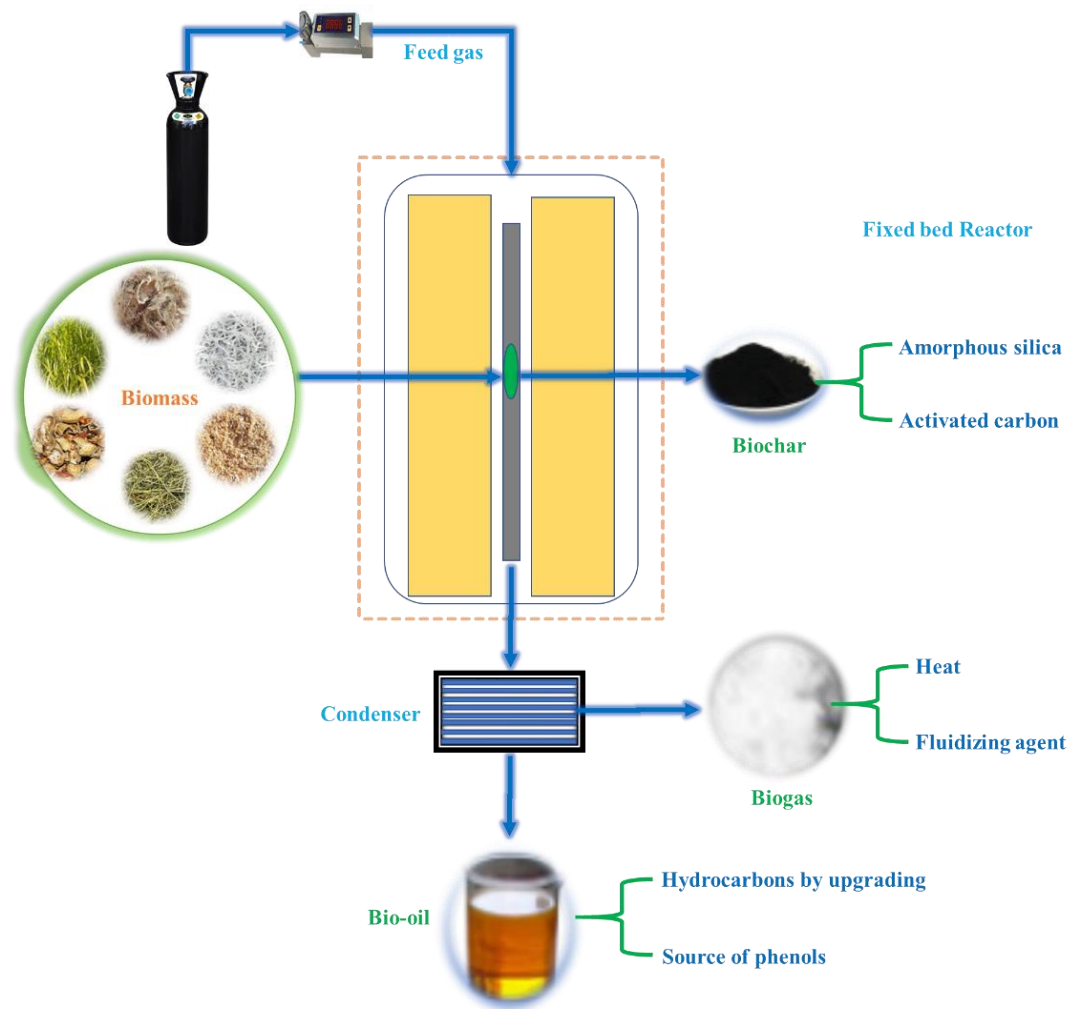


**Figure 2-3** Pyrolysis of biomass in a fixed bed reactor to produce valuable goods (self-created)

## 2.3 Co-pyrolysis

Biomass co-pyrolysis is becoming popular as a feasible alternative method for improving the quality of pyrolysis products. In contrast to basic biomass quick pyrolysis, co-pyrolysis uses various raw materials for feedstock along with biomass, such as plastics, coal, sludge, tyres, and so on. Co-pyrolysis is a unique trait because of the synergistic influence between the chemical reactions between different feedstocks. However, depending on the extra raw materials employed in co-pyrolysis, the synergistic effect varies significantly.

As a result, coal and biomass co-pyrolysis might give liquid along with gaseous products with significant economic worth, exceeding the constraints of individual coal and biomass pyrolysis [29]. Biomass could give hydrogen during the process, swiftly producing volatile compounds in significant volume, possibly enhancing gas-lignite contact will lead to changes in product distribution, kinetics, and tar and gas composition, as well as improved char gasification and interaction with the gaseous phase during secondary tar cracking. Incorporating biomass into coal is a feasible strategy for lowering our dependency on fossil fuels while simultaneously addressing the environmental difficulties posed by CO<sub>2</sub> emissions from coal; CO<sub>2</sub> emissions are the second major contributor to global warming [30]. The study of co-pyrolysis is a disputed subject. Its primary purpose is to improve the thermal transformation of coal. The majority of previous research [31-33] has shown little evidence of a synergistic effect between coal and biomass. Recent research [34-37] has revealed the importance of co-pyrolysis interactions in TGA. Other studies [38, 39] have found a synergistic effect on pyrolytic product yields, gaseous component yields, tar component yields, and char reactivities. Table 2-2 illustrates the results of past coal and biomass co-pyrolysis research. Because of its high energy density and low cost, coal is a good fuel for biomass co-pyrolysis. Alkali and alkaline-earth metals in biomass, as well as hydrogen donors, influence the co-pyrolysis process. There is still a need for research into the synergistic effects that occur when biomass and coal are combined.

**Table 2-2** Literature on coal-biomass studies

<b>Feedstock</b>	<b>Biomass (wt. %) in the blend</b>	<b>Flowrate (mL/min)</b>	<b>Heating rate (°C/min)</b>	<b>Temperature (°C)</b>	<b>Ref.</b>
Rice straw/ bituminous coal	4/8/12/16/32	N <sub>2</sub> /500	NA	700–900	[29]
Sawdust/ bituminous coal	20/40/60/80	N <sub>2</sub> /500	NA	800–1400	[40]
Pine sawdust, legume straw/brown, bituminous coal	0–100	N <sub>2</sub> /35	8.3	500–700	[38]
Rice husk/ Bituminous coal	0/20/40/60/100	N <sub>2</sub>	10–30	900	[41]
Sugarcane bagasse/ Bituminous coal	20/40/60/80	N <sub>2</sub>	10	25–1100	[42]
Pine/sub-bituminous coal	0–100	N <sub>2</sub>	NA	600	[43]
sugarcane bagasse/ Coal	10/20/30/40/50	N <sub>2</sub>	20	25–900	[44]

### **2.3.1 Synergistic effect**

Biomass-coal mix interaction was studied by comparing experimental data to theoretical data, which is the total of each sample value in proportion to their blending value. Synergistic effects are the percentage increase or reduction in experimental results relative to theoretical values. Some groups' findings may be inconsistent since there are so many factors to consider. In other words, co-pyrolysis procedures using biomass and coal have shown synergistic or cumulative effects. Using thermogravimetric analysis (TG), no synergistic effect was found in the pyrolysis of coal-biomass blends in various coal and biomass ratios, and the char production and the amount of biomass in the blend were shown to have a linear relationship[33]. Kastanaki et al. [45] and Pan et al. [46] Kastanaki et al. [45] both confirmed that biomass and coal in a blend did not interact during pyrolysis. Aboyade et al. [47], Chen et al.[36] , Shui et al. [37], have challenged this perspective, demonstrating that during pyrolysis in TGA, extensive interactions between the coal and biomass fractions occur.. Sonobe et al. [32], Onay et al. [35], and Li et al. [40] stated that the yields of pyrolysis goods, tar, gaseous, and char component, all confirmed the presence of a synergistic effect. Park et al. [48] found the interaction in both fixed-bed reactors and TG, however, Sonobe et al. [32], who investigated the co-pyrolysis of corncob and lignite, found that synergy occurs in a fixed bed reactor instead of TG device. Furthermore, studies that look at the distribution of key products like char, gas, and liquid tried to find little indication of a synergistic effect [49], those who examine the volatiles' composition, on the other hand, are more likely to reach the opposite conclusion [50]. It's challenging to verify synergy in co-pyrolysis because it depends on type of fuels and the pyrolysis technique employed. These opposing results are puzzling and need to be clarified. Individual studies on coal and biomass pyrolysis have resulted in a flood of reviews [51, 52]. Instead of this, there are few reviews on the co-pyrolysis of coal-biomass blends [53].

## **2.4 Co-pyrolysis parameters and synergistic effect**

### **2.4.1 Feedstock type**

The main component that might entice the synergy should be the types of blending fuels. Many coal-biomass blends, such as hazelnut shells-coal, have been demonstrated to be effective [54], sawdust-coal [55], legume straw-coal [38], corncob-coal [32], microalgae-coal [32], and corn stalk-sub-bituminous coal [56], show synergetic effects during co-pyrolysis. Hemicellulose, cellulose, and lignin have various extractives, and minerals are primary chemical components of biomass. Cellulose, hemicellulose, and lignin may have additive impacts on coal's thermal behavior [57]. The OH and H functional groups of biomass accelerate the cracking of coal's aromatic rings in co-pyrolysis [58, 59]. Some studies also stated that biomass natural resources encouraged interaction between coal and biomass [60]. According to Yuan et al. [61], the greatest enhancement of hemicellulose effect on coal cracking and conversion in co-pyrolysis. The volatiles produced by pyrolysis are principally caused by the hemicellulose and cellulose elements of biomass, which can subsequently be used to manufacture hydrogen through secondary processes. Lignin in biomass may facilitate polymerizing processes at low temperatures, resulting in the formation of reactive radicals and stabilized phenoxy radicals [62, 63].

Many studies have found that biomass and low-rank coals may readily develop synergy during co-pyrolysis, and that interactions are greater than interactions in high-rank coal and biomass [54, 61, 64, 65]. Furthermore, when coal rank is low, the main pyrolytic zones moved to lower temperatures [66]. Instantaneously, in low rank coal hydrogen acceptor ability was superior to that of high ranked coal [67]. During the process, structures of the coal will be broken, resulting in considerable coal fragmentation into hydrogen with no active sites. A hydrogen transfer process occurs between biomass and coal. Low-rank coals have a higher potential for hydrogen uptake; therefore, the synergistic beneficial effect is more noticeable.

#### **2.4.2 Blending ratio**

Liquid, solid, and gas product distributions were significantly influenced by the blend's biomass content [50]. The char yield is reduced, but the gas and liquid yields are increased by raising the blending ratio [43, 56]. According to co-pyrolysis research on

TG, the RL percentage in blends fell as the biomass quantity in the blends rose. [36, 41, 68]. For coal-biomass blends, the TGA bends are exposed in Figure 2-4. Coal's solid phase is mostly composed of aromatics ring [50]. Biomass decompose more quickly as compared to coal. Figure 2-4 shows that the curve for the blends was in the central of curves for the individual components, as biomass loses more weight than coal. Changing the biomass blending percentage in coal-biomass blends can also modify the ignition and peak decomposition temperatures. Other breakdown features, such as weight loss and residue remaining, are mostly influenced by the blending ratio. In most research, biomass results in the greatest weight loss when compared to coal.

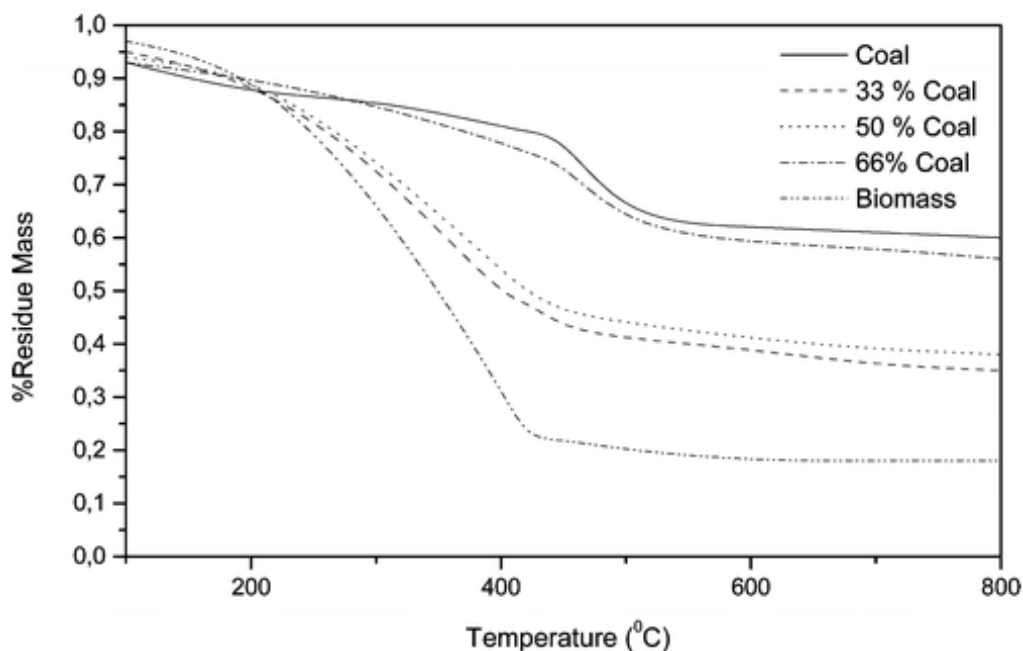


**Figure 2-4** Residue mass vs the temperature for coal-biomass blends [69]

However, some studies [38, 70] stated that the amount of biomass in the blends had no influence on the degree of synergistic effect because biomass has a lower thermal conductivity packing density as compared to coal, increasing the amount of biomass in the blend would slow the heating rate and cause the volatiles from both coal and biomass to take longer to be released [48]. As a result, biomass H and OH radicals are released slowly, enhancing coal tar cracking [32, 37]. Furthermore, biomass char residues formed during co-pyrolysis easily build on coal molecules, inhibiting the cracks by which the

volatile material produced by coal pyrolysis is released. Pyrolysis of biomass produced hydrogen-rich gas [53].

### **2.4.3 Heating rate**

The temperature decomposition for coal and biomass pyrolysis is mostly different, if the heating rate is slow then it is difficult to observe synergistic effects [71]. It's feasible that the pyrolysis of blends might happen at high heating rate, resulting in a volatile emission overlap from both coal and biomass [38]. Because the reaction atmosphere also contains non-inert species, coal pyrolysis yields and products may differ at high heating rates [72]. Co-pyrolysis of coal-biomass blends at high heating rates, in other words, favored synergism [39, 61, 73].

Biomass and coal are devolatilized together in an inert atmosphere when co pyrolysis, resulting in a combined solid char and volatile stream as results. As a result, the synergistic effect seen during co-pyrolysis could be attributed to volatile-char and volatile-volatile interactions [74, 75]. The generation of greater yields of volatile was aided by a faster heating rate [71, 76]. The possibility of gas phase reactions in biomass and coal volatiles increase by adopting these parameters, hence increasing the synergism's intensity [77, 78].

### **2.4.4 Operating temperature**

The pyrolysis temperature has a substantial influence on the product distribution of coal-biomass blends, according to a literature search and previous experiments [38, 39, 48]. The coal pyrolysis produces mostly solids with minor amount of gases and liquid, while the biomass pyrolysis produces solid, gaseous, and liquid products. The obtained products from coal-biomass co pyrolysis is relatively same as both individual fuels. However, the synergistic effect affected them to diverge from the estimated amount of product [32].

Char yield reduced and the volatiles yield increase as the temperature increased [48]. Therefore, when the temperature rose, the conversion of pyrolysis increased. Many

researchers believe that at low temperature biomass can help to devolatilize coal [79], The indications of coal-biomass synergy, strongly depending on reaction temperature. The synergistic effect mostly happened in 300-500°C, according to Aboyade et al. [47], conforming to the beginning of coal breakdown and end of biomass devolatilization. There is synergy between secondary processes in the blends, according to Ulloa et al. [78], Synergy between coal pyrolysis and sawdust in the production of volatiles is strongest around 400°C. According to Park et al. [48] when the ratio of biomass was 0.6 at a temperature of 600°C, synergistic effects result in the generation of additional volatiles in a fixed bed under isothermal conditions between 500°C and 700°C. For co-pyrolysis of biomass and coal mix at 600°C, is the best temperature, where considerable free radical and hydrogen donors are formed [38]. As a result, the ideal temperature range for synergy occurrence is 400–600°C. Several scholars have said that [32, 48], as the temperature increases up to 800°C, the discrepancy in the experimental and estimated yields reduce.

#### **2.4.5 The reactor types**

The performance of co-pyrolysis process has been studied through various reactors, including fixed-bed reactors, TGA, drop style high frequency magnetic field-based furnaces, fluidized bed reactors, and free-fall reactors [59, 72, 80, 81]. In TGA lack of synergetic effect are present due to lower heating rate is used that allow the several devolatilization stages of together fuel in the mixture to be certainly divided. Moreover, the flow rate of nitrogen is high enough that may prevent volatiles to remaining near to the devolatilizing elements in the vessel. Therefore, the major reasons for the absence of interactions are the attempts to maintain an inactive environment [72]. However, many researchers have all disputed this idea, demonstrating that in TGA significant synergistic effect is observed during coal-biomass blends co-pyrolysis [36, 47, 78]. Previously Table 2-2 summaries of existing literature on co pyrolysis in TGA. Close interaction between nearby fuel particles and associated volatiles would be possible in fixed bed reactors with large sample volumes, resulting in a synergistic effect for both gas product compositions and pyrolysis product generation [60, 82, 83]. However, close contact in coal and biomass particles during co-pyrolysis not always imply the presence of interaction [84]. The

vacuum pyrolysis and pressurized pyrolysis of coal-biomass blends confirmed the existence of synergistic effect, when compared to atmospheric fixed-bed reactors [50, 85]. The tube furnaces used for pyrolysis, on the other hand, typically feature extensive high temperature zones, and before escaping from the reactors the volatiles pass through this zone. To increase secondary reactions for char formation and tar cracking is possible by increasing residence time of intraparticle volatiles. [86]. As a result, it's impossible to tell whether the synergies in these reactors are mostly due to the second volatile reaction or the initial pyrolysis process [59].

Many different types reactor have been constructed for co-pyrolysis products that operate at fast heating rate. The Fluidized-bed reactors, according to some researchers, are not suited for studying interactions because the sample particles are completely separated in this setup, that cause lack in synergistic effect during co-pyrolysis [60]. Xu et al. [43] In a free-fall reactor, researchers investigated coal-biomass blends co-pyrolysis and discovered that a higher blending ratio of about 70% and a lower temperature of around 600°C are more favorable to synergistic effects. Certain specially constructed reactors, such as a micro fluidized bed reactor, a single-particle reactor system, and congruent mass TGA, have been used to investigate the co-pyrolysis behavior of coal-biomass blends [84, 87, 88].

## **2.5 Thermo-Kinetics Analysis**

### **2.5.1 Kinetic modeling overview**

Pyrolysis is an effective and reliable way to make bio-oil, charcoal, and producing gas all in one step. Producer gas is a gaseous fuel that may be used to power a gas turbine as well as to heat a building. As a result, calculating bioenergy product yields requires a thorough understanding of the pyrolysis mechanism. As a result, the only way to estimate it is to simulate the pyrolysis mechanism. The TGA method analyses the mass change of a sample as a function of time. A kinetic study should be performed before converting biomass to fuel to obtain valuable information for constructing pyrolysis reactors and

improving the process parameters [89, 90]. Due to changes in composition, different feedstock's exhibit varied thermal behavior profiles [91].

The solid-state materials pyrolysis, such as biomass and coal is contain a heterogeneous chemical reaction. Three essential components, interfacial diffusion of reactants and products, changing reaction geometry, and breakdown and redistribution of chemical bonds, can alter the chemical kinetics and reaction dynamics of heterogeneous processes [92]. Unlike homogeneous reactions, concentration is a useless measure that can't be used to follow the evolution of heterogeneous reaction kinetics since it fluctuates spatially [92-94]. The adsorption, nucleation, interfacial reaction, desorption, and surface or bulk diffusion are examples of heterogeneous reactions that typically include a superposition of many primary processes [94]. In solid-state decomposition reactions, the initiation step usually involves a “random walk” of vacancies and defects inside the crystal-lattice that resulting in nucleation growth [95]. Also, the reaction interface, which is defined as the boundary surface between the product and reactant. This concept is commonly used to simulate solid state reaction kinetics [94].

### **2.5.2 Model fitting and model free overview**

A variety of models and methodologies were used to investigate pyrolysis kinetics. Model-fitting method provide helpful information about reaction mechanism involve in pyrolysis and determination of  $E_a$  [96, 97]. For estimating the apparent  $E_a$  for fixed mass conversions, model-free method are also a reliable method [91]. Based on the calculated kinetic triplet such as  $E_a$ , and  $A$ , and mechanism function, a major way to explore the thermal degrading process of biomass is currently extensively employed [98]. Non-isothermal approaches for determining kinetics had the benefit of executing the temperature program more rapidly and readily than isothermal methods [99].

Table 2-3 presents the most frequent models used in the evaluation of kinetics parameters and discusses the assumption that has been made to perform these models. The model free and model fitting methods were employed in the non-isothermal kinetics. The two model free methods are the Kissinger Akahira Sunose (KAS) [100] and Flynn Wall

Ozawa (FWO) [101] method, that assuming the reaction rate was only dependent on the reaction temperature for a fixed conversion. Various heating rate were used instead of a single heating rate without information of the reaction mechanism to calculate more reliable kinetic parameters. The mode fitting technique, on the other hand, was developed using a specific reaction mechanism such as diffusion, order-based, or power-law models to depict the conversion reliance on the reaction rate [94, 102]. The most crucial step in using a mode-fitting approach, such as in Coats Redfern [103] method, was to find an adequate reaction mechanism that describe degradation of sample [104]. Therefore, both methods have pros and cons. The combined, can obtain not only the  $E_a$ , and A but also find the most probable reaction mechanism [105]. Vyazovkin et al. [106] believe that the kinetic parameters attained by model free methods are more accurate and consistent. The model free procedures provide less specific information than model fitting methods [107, 108].

**Table 2-3** Comprehensively used model fitting and model free methods, general forms, and assumption [109]

Kinetic Models	Formulation	Rules	Plotting variables
Coats-Redfern (integral method)	$n = 1, \ln \left[ -\frac{\ln(1 - \alpha)}{T^2} \right] = \ln \left[ \frac{AR}{\beta E} \left( 1 - \frac{2RT}{E} \right) - \frac{E}{RT} \right]$ $n \neq 1, \ln \left[ -\frac{1 - (1 - \alpha)^{1-n}}{T^2(1 - n)} \right] = \ln \left[ \frac{AR}{\beta E} \left( 1 - \frac{2RT}{E} \right) - \frac{E}{RT} \right]$	Uses Taylor series and assumes the value of the reaction order.	$\ln \frac{[g(\alpha)]}{T^2} \text{ vs } \left( \frac{1}{T} \right),$ $\text{Slope} = -\frac{E}{R}$ $\text{Intercept} = \ln \left( \frac{AR}{\beta E} \right)$
KAS method (integral and Iso-conversional)	$\log p(x) \cong \frac{\exp^{-x}}{x^2}, \text{ for } 20 \leq x \leq 50$	T <sub>m</sub> : temp. At max reaction rate Assumes conversion is fixed.	$\ln \left( \frac{\beta}{T_m^2} \right) \text{ vs } \left( \frac{1}{T_m} \right)$ $\text{Slope} = E$
Friedman Method (differential Iso conversional)	$\ln \left( \frac{d\alpha}{dt} \right) = \ln \left[ \beta \left( \frac{d\alpha}{dt} \right) \right] = \ln [Af(\alpha)] - \frac{E}{RT}$ <p>Rearranging by using Doyle's approximation gives, <math>\ln \left( \frac{\beta}{T_m^2} \right) = -\frac{E}{R} \left( \frac{1}{T_m} \right) - \ln \left[ \left( \frac{E}{AR} \right) \int_0^\alpha \frac{d\alpha}{f(\alpha)} \right]</math></p>	Assumes f(α) constant. Degradation is depending only on the rate of mass loss and independent of temperature.	$\ln \left( \frac{d\alpha}{dt} \right) \text{ vs } \left( \frac{1}{T} \right)$ $\text{Slope} = -\frac{E}{R}$

### 2.5.2.1 Coats Redfern method

To examine the validity of model fitting methods and provide the most appropriate reaction model for biomass decomposition, the Coats Redfern approach is used. The Arrhenius equation is used in this model-based strategy. The Coats Redfern method is used to explore the  $E_a$  and  $A$  of complicated compounds with great success [110, 111]. The most extensively used strategies for determining reaction mechanisms is attain by Coat Redfern methods. Zakrzewski et al. [112] studied biomass kinetics in a non-isothermal situation at a heating rate of 5 °C/min by using Coats Redfern method and conclude that the  $E_a$  and  $A$  were 93.1-174.9 kJ/mol and 4.9104-7.11011 1/min, respectively. Reina et al. [113] used TGA under isothermal conditions to explore the kinetics of forest wood and ancient furniture and found  $E_a$  and  $A$  values were in range 215.7-127.8 kJ/mol and 1.89107–3.40107 s<sup>-1</sup>, respectively. Using the Coats Redfern method, B. Nyoni et al. [114] explore the co-pyrolysis kinetics behavior of bituminous coal and microalgae. The activation energy of coal was 81.8 kJ/mol during the first stage and 649.3 kJ during the second stage, whereas microalgae activation energy was 145.5 kJ/mol and 127.3 kJ/mol during the first and second stages, respectively. Coats Redfern technique was used to examine co-pyrolysis and co-combustion kinetics on coal-biomass blends by Jian Wang et al. and co-authors [115]. Their results showed that blending ratio of biomass in blend affects the  $E_a$  and  $A$ . In literature, L. F. Madiedo et al. [116] found kinetic parameters (Friedman, KAS, and FWO), and the reaction mechanism for decomposition was discovered using the Coats Redfern method during co-pyrolysis of coal, terrified sawdust, and paraffin. Hence, Coats Redfern method has been widely used in kinetics for solid materials decomposition [117].

### 2.5.3 Thermodynamics parameters

Thermodynamics parameters such as  $\Delta H$ ,  $\Delta G$ , and  $\Delta S$  are important parameters that may be derived using kinetics parameters ( $E_a$ ,  $A$ , and peak decomposition temperature  $T_p$ ) [118]. Thermodynamic parameters are equally significant as kinetic parameters in reactor design and scaling. The thermodynamics parameters validate whether a process is possible to occur or not. The  $\Delta H$  depicted the endothermic and exothermic behavior of processes.

The  $\Delta H$  illustrates the energy changes in the reagents and activated complex. If the low energy barrier, the activation of the complex is preferred [119]. Furthermore, the high  $\Delta H$  values, indicate stronger structural heat resistance, which could be owing to a smaller level of (positive) synergistic interactions [120]. The  $\Delta G$  denotes the system's overall energy increase as it approaches reagent equilibrium and the creation of an activated complex [121].

The positive  $\Delta G$  values imply that the system requires an external energy because the process is non-spontaneous. The value  $\Delta S$  indicates how far or close the system is in achieving its thermodynamic equilibrium [120]. The low  $\Delta S$  value suggests that the material has undergone some chemical or physical change, that bringing it close to its thermodynamic equilibrium [122]. The thermodynamics parameter of acai seed biomass during pyrolysis was determined by Vanuza O. Santos et al. [123] who found that the value of  $\Delta H$  was 154.298 kJ/mol, the value of  $\Delta G$  was 148.76 kJ/mol, and the value of  $\Delta S$  was positive. Also, during the sewage sludge-and rice husk co-pyrolysis, S. R. Naqvi et al. [118] also discovered the thermodynamics parameter.

The results revealed that the  $\Delta H$  reaction mechanism exhibited both exothermic and endothermic behavior, and the  $\Delta G$  was positive for all samples, although the  $S$  values were negative for all samples. A study on sewage sludge-HDPE co-pyrolysis was undertaken by A. Zaker et al. [124]. The findings of thermodynamic parameters showed that the  $\Delta H$  values of a 50 percent sewage sludge mix were 194.56-206.44 kJ/mol and the  $\Delta G$  values were 119.28-119.54 kJ/mol, showing that bioenergy production is viable.

## Summary

Fossil fuels reserves depletion and harmful emissions necessity to be addressed on an urgent basis to partially save their reserves and reduce climate change. Among fossil fuels, coal reserves will be available up to the next 200 years, but their emissions cause thoughtful damage. However, coal can be used efficiently by various processing techniques such as pyrolysis, gasification, etc. Pyrolysis of coal is a good option to produce synthesis fuels to reduce emissions. However, the yield of the products is low because coal has a low H/C ratio.

As an alternative of coal, a biomass pyrolysis is an interesting option because it is a renewable, broadly available, and CO<sub>2</sub> neutral organic material. These all products are the sustainable source for energy production, but the calorific value of the product is relatively low as compared to coal. Moreover, bio-oil from biomass pyrolysis contains high moisture and oxygenated compound which may cause problems such as fouling, slagging, and corrosion. Therefore, the coal-biomass blend co-pyrolysis is a suitable option because biomass contains high hydrogen content which will support in coal pyrolysis. Additionally, the calorific value of products will increase due to coal blending. Coal-biomass blending is supportive in partially saving of coal reserves. However, there is a need to characterize coal-biomass blends to evaluate their co-pyrolysis behaviour. For this drive, various characterizations are used. The synergistic effect or the yield of co-pyrolysis product depends on reaction parameters.

The kinetic study helps in judgement of an appropriate reaction mechanism for thermal degradation of coal-biomass blends. It will further be supportive in designing and scaling of co-pyrolysis reactor Coats Redfern's method approaches the most suitable reaction mechanism by modelling various integral functions. Furthermore, the thermodynamic parameters are derived from the kinetic parameter that gives the  $\Delta H$ ,  $\Delta G$ , and  $\Delta H$ . These parameters are important in the understanding of the co-pyrolysis process.

## References

1. Oberschelp, C., et al., *Global emission hotspots of coal power generation*. 2019. **2**(2): p. 113-121.
2. Oliveira, M.L., et al., *Multifaceted processes controlling the distribution of hazardous compounds in the spontaneous combustion of coal and the effect of these compounds on human health*. 2018. **160**: p. 562-567.
3. Lozano, R., et al., *Measuring progress from 1990 to 2017 and projecting attainment to 2030 of the health-related Sustainable Development Goals for 195 countries and territories: a systematic analysis for the Global Burden of Disease Study 2017*. 2018. **392**(10159): p. 2091-2138.
4. Wagner, N.J., *Geology of Coal*, in *Encyclopedia of Geology (Second Edition)*, D. Alderton and S.A. Elias, Editors. 2021, Academic Press: Oxford. p. 745-761.
5. Council, W.E.J.W.E.C., London, UK, *World energy resources 2016*. 2016.
6. Agreement, P. *Paris agreement*. in *Report of the Conference of the Parties to the United Nations Framework Convention on Climate Change (21st Session, 2015: Paris)*. Retrived December. 2015. HeinOnline.
7. Hendryx, M., et al., *Air pollution emissions 2008–2018 from australian coal mining: Implications for public and occupational health*. 2020. **17**(5): p. 1570.
8. Oliveira, M.L., et al., *Study of coal cleaning rejects by FIB and sample preparation for HR-TEM: mineral surface chemistry and nanoparticle-aggregation control for health studies*. 2018. **188**: p. 662-669.
9. World Health Organization %J World Health Organization: Geneva, S., *WHO global ambient air quality database (update 2018)*. 2018.
10. Gasparotto, J. and K. Da Boit Martinello, *Coal as an energy source and its impacts on human health*. *Energy Geoscience*, 2021. **2**(2): p. 113-120.
11. Zhang, H., S. Fu, and Y.J.I.j.o.b.m. Chen, *Basic understanding of the color distinction of lignin and the proper selection of lignin in color-depended utilizations*. 2020. **147**: p. 607-615.
12. Iglauer, S., et al., *Hydrogen Adsorption on Sub-Bituminous Coal: Implications for Hydrogen Geo-Storage*. 2021. **48**(10): p. e2021GL092976.
13. Xiao, Y., et al., *Influence of element composition and microcrystalline structure on thermal properties of bituminous coal under nitrogen atmosphere*. 2021. **147**: p. 846-856.
14. Liu, J., et al., *Molecular characterization of Henan anthracite coal*. 2019. **33**(7): p. 6215-6225.
15. Miura, K., *Mild conversion of coal for producing valuable chemicals*. *Fuel Processing Technology*, 2000. **62**(2): p. 119-135.
16. Abnisa, F. and W.M.A. Wan Daud, *A review on co-pyrolysis of biomass: An optional technique to obtain a high-grade pyrolysis oil*. *Energy Conversion and Management*, 2014. **87**: p. 71-85.
17. Kammen, D.M., *Renewable Energy, Taxonomic Overview*, in *Encyclopedia of Energy*, C.J. Cleveland, Editor. 2004, Elsevier: New York. p. 385-412.
18. Irfan, M., et al., *Assessing the energy dynamics of Pakistan: prospects of biomass energy*. 2020. **6**: p. 80-93.

19. Kumar, N. and A. Dixit, *Chapter 4 - Management of biomass*, in *Nanotechnology for Rural Development*, N. Kumar and A. Dixit, Editors. 2021, Elsevier. p. 97-140.
20. Mudgil, D., *Chapter 3 - The Interaction Between Insoluble and Soluble Fiber*, in *Dietary Fiber for the Prevention of Cardiovascular Disease*, R.A. Samaan, Editor. 2017, Academic Press. p. 35-59.
21. Calvo-Flores, F.G., *Lignin: A Renewable Raw Material*, in *Encyclopedia of Renewable and Sustainable Materials*, S. Hashmi and I.A. Choudhury, Editors. 2020, Elsevier: Oxford. p. 102-118.
22. Zhao, S.-X., N. Ta, and X.-D. Wang, *Effect of Temperature on the Structural and Physicochemical Properties of Biochar with Apple Tree Branches as Feedstock Material*. *Energies*, 2017. **10**(9).
23. Chen, D., et al., *Investigation of biomass torrefaction based on three major components: Hemicellulose, cellulose, and lignin*. 2018. **169**: p. 228-237.
24. Hu, X. and M. Gholizadeh, *Biomass pyrolysis: A review of the process development and challenges from initial researches up to the commercialisation stage*. *Journal of Energy Chemistry*, 2019. **39**: p. 109-143.
25. Zhang, S., et al., *High quality syngas production from microwave pyrolysis of rice husk with char-supported metallic catalysts*. 2015. **191**: p. 17-23.
26. Luo, H., et al., *Low temperature microwave-assisted pyrolysis of wood sawdust for phenolic rich compounds: Kinetics and dielectric properties analysis*. 2017. **238**: p. 109-115.
27. Jun, Z., et al., *Hydrogen-rich syngas produced from the co-pyrolysis of municipal solid waste and wheat straw*. 2017. **42**(31): p. 19701-19708.
28. Zhao, X., et al., *Microwave pyrolysis of corn stalk bale: A promising method for direct utilization of large-sized biomass and syngas production*. 2010. **89**(1): p. 87-94.
29. Li, S., et al., *Study on co-pyrolysis characteristics of rice straw and Shenfu bituminous coal blends in a fixed bed reactor*. *Bioresource Technology*, 2014. **155**: p. 252-257.
30. Hassan, H., J.K. Lim, and B.H. Hameed, *Recent progress on biomass co-pyrolysis conversion into high-quality bio-oil*. *Bioresource Technology*, 2016. **221**: p. 645-655.
31. Vuthaluru, H.B., *Thermal behaviour of coal/biomass blends during co-pyrolysis*. *Fuel Processing Technology*, 2004. **85**(2): p. 141-155.
32. Sonobe, T., N. Worasuwannarak, and S. Pipatmanomai, *Synergies in co-pyrolysis of Thai lignite and corncob*. *Fuel Processing Technology*, 2008. **89**(12): p. 1371-1378.
33. Vuthaluru, H.B., *Thermal behaviour of coal/biomass blends during co-pyrolysis*. *Fuel processing technology*, 2004. **85**(2-3): p. 141-155.
34. Zhang, L., et al., *Influence of woody biomass (cedar chip) addition on the emissions of PM10 from pulverised coal combustion*. *Fuel*, 2011. **90**(1): p. 77-86.
35. Onay, Ö., E. Bayram, and Ö.M. Koçkar, *Copyrolysis of seytömer– lignite and safflower seed: influence of the blending ratio and pyrolysis temperature on product yields and oil characterization*. *Energy & fuels*, 2007. **21**(5): p. 3049-3056.

36. Chen, C., X. Ma, and Y. He, *Co-pyrolysis characteristics of microalgae Chlorella vulgaris and coal through TGA*. Bioresource Technology, 2012. **117**: p. 264-273.
37. Shui, H., et al., *Co-liquefaction behavior of a sub-bituminous coal and sawdust*. Energy, 2011. **36**(11): p. 6645-6650.
38. Zhang, L., et al., *Co-pyrolysis of biomass and coal in a free fall reactor*. Fuel, 2007. **86**(3): p. 353-359.
39. Yuan, S., et al., *Rapid co-pyrolysis of rice straw and a bituminous coal in a high-frequency furnace and gasification of the residual char*. Bioresource Technology, 2012. **109**: p. 188-197.
40. Li, S., et al., *Co-pyrolysis behaviors of saw dust and Shenfu coal in drop tube furnace and fixed bed reactor*. Bioresource Technology, 2013. **148**: p. 24-29.
41. Li, S., et al., *Co-pyrolysis characteristic of biomass and bituminous coal*. Bioresource Technology, 2015. **179**: p. 414-420.
42. Strydom, C.A., et al., *The influence of selected biomass additions on the co-pyrolysis with an inertinite-rich medium rank C grade South African coal*. Journal of the Southern African Institute of Mining and Metallurgy, 2015. **115**: p. 707-716.
43. Quan, C., et al., *Co-pyrolysis of biomass and coal blend by TG and in a free fall reactor*. Journal of Thermal Analysis and Calorimetry, 2014. **117**(2): p. 817-823.
44. Mortari, D.A., I. Ávila, and P.M. Crnkovic. *Co-firing study of sugar cane bagasse and coal applying thermogravimetric analysis and kinetic*. in *In Proceedings of the International Congress of Mechanical Engineering-COBEM*.
45. Kastanaki, E., et al., *Thermogravimetric studies of the behavior of lignite–biomass blends during devolatilization*. Fuel processing technology, 2002. **77**: p. 159-166.
46. Pan, Y.G., E. Velo, and L. Puigjaner, *Pyrolysis of blends of biomass with poor coals*. Fuel, 1996. **75**(4): p. 412-418.
47. Aboyade, A.O., et al., *Thermogravimetric study of the pyrolysis characteristics and kinetics of coal blends with corn and sugarcane residues*. Fuel Processing Technology, 2013. **106**: p. 310-320.
48. Park, D.K., et al., *Co-pyrolysis characteristics of sawdust and coal blend in TGA and a fixed bed reactor*. Bioresource Technology, 2010. **101**(15): p. 6151-6156.
49. Moghtaderi, B., C. Meesri, and T.F. Wall, *Pyrolytic characteristics of blended coal and woody biomass*. Fuel, 2004. **83**(6): p. 745-750.
50. Aboyade, A.O., et al., *Slow and pressurized co-pyrolysis of coal and agricultural residues*. Energy Conversion and Management, 2013. **65**: p. 198-207.
51. Collard, F.-X. and J. Blin, *A review on pyrolysis of biomass constituents: Mechanisms and composition of the products obtained from the conversion of cellulose, hemicelluloses and lignin*. Renewable and Sustainable Energy Reviews, 2014. **38**: p. 594-608.
52. Lédé, J., *Cellulose pyrolysis kinetics: An historical review on the existence and role of intermediate active cellulose*. Journal of Analytical and Applied Pyrolysis, 2012. **94**: p. 17-32.
53. Quan, C. and N. Gao, *Copyrolysis of biomass and coal: a review of effects of copyrolysis parameters, product properties, and synergistic mechanisms*. BioMed research international, 2016. **2016**.

54. Haykiri-Acma, H. and S. Yaman, *Interaction between biomass and different rank coals during co-pyrolysis*. Renewable Energy, 2010. **35**(1): p. 288-292.
55. Lee, J.-Y., et al., *Comparison of several methods for effective lipid extraction from microalgae*. Bioresource Technology, 2010. **101**(1, Supplement): p. S75-S77.
56. Guo, M. and J.-C. Bi, *Characteristics and application of co-pyrolysis of coal/biomass blends with solid heat carrier*. Fuel Processing Technology, 2015. **138**: p. 743-749.
57. Wu, Z., et al., *Synergistic effect on thermal behavior during co-pyrolysis of lignocellulosic biomass model components blend with bituminous coal*. Bioresource Technology, 2014. **169**: p. 220-228.
58. Blesa, M.J., et al., *Low-temperature co-pyrolysis of a low-rank coal and biomass to prepare smokeless fuel briquettes*. Journal of Analytical and Applied Pyrolysis, 2003. **70**(2): p. 665-677.
59. Jones, J.M., et al., *Devolatilisation characteristics of coal and biomass blends*. Journal of Analytical and Applied Pyrolysis, 2005. **74**(1): p. 502-511.
60. Collot, A.G., et al., *Co-pyrolysis and co-gasification of coal and biomass in bench-scale fixed-bed and fluidised bed reactors*. Fuel, 1999. **78**(6): p. 667-679.
61. Yuan, S., et al., *Nitrogen conversion under rapid pyrolysis of two types of aquatic biomass and corresponding blends with coal*. Bioresource Technology, 2011. **102**(21): p. 10124-10130.
62. Jongwon Kim, S.B.L.C.B.M.B.A.A., *Coliquefaction of Coal and Black Liquor to Environmentally Acceptable Liquid Fuels*. Energy Sources, 1999. **21**(9): p. 839-847.
63. Lalvani, S.B., et al., *Coal liquefaction in lignin-derived liquids under low severity conditions*. Fuel, 1991. **70**(12): p. 1433-1438.
64. Haykiri-Acma, H. and S. Yaman, *Synergy in devolatilization characteristics of lignite and hazelnut shell during co-pyrolysis*. Fuel, 2007. **86**(3): p. 373-380.
65. Suelves, I., M.J. Lázaro, and R. Moliner, *Synergetic effects in the co-pyrolysis of samca coal and a model aliphatic compound studied by analytical pyrolysis*. Journal of Analytical and Applied Pyrolysis, 2002. **65**(2): p. 197-206.
66. Kastanaki, E. and D. Vamvuka, *A comparative reactivity and kinetic study on the combustion of coal–biomass char blends*. Fuel, 2006. **85**(9): p. 1186-1193.
67. Kidena, K., S. Murata, and M. Nomura, *Studies on the Chemical Structural Change during Carbonization Process*. Energy & Fuels, 1996. **10**(3): p. 672-678.
68. Meng, H., et al., *Thermal behavior and the evolution of char structure during co-pyrolysis of platanus wood blends with different rank coals from northern China*. Fuel, 2015. **158**: p. 602-611.
69. Onay, Ö., E. Bayram, and Ö.M. Koçkar, *Copyrolysis of Seyitömer–Lignite and Safflower Seed: Influence of the Blending Ratio and Pyrolysis Temperature on Product Yields and Oil Characterization*. Energy & Fuels, 2007. **21**(5): p. 3049-3056.
70. Aboyade, A.O., et al., *Model fitting kinetic analysis and characterisation of the devolatilization of coal blends with corn and sugarcane residues*. Thermochemica Acta, 2012. **530**: p. 95-106.
71. Meesri, C. and B. Moghtaderi, *Lack of synergetic effects in the pyrolytic*

- characteristics of woody biomass/coal blends under low and high heating rate regimes.* Biomass and Bioenergy, 2002. **23**(1): p. 55-66.
72. Biagini, E., et al., *Devolatilization rate of biomasses and coal–biomass blends: an experimental investigation.* Fuel, 2002. **81**(8): p. 1041-1050.
  73. Yuan, S., et al., *HCN and NH<sub>3</sub> Released from Biomass and Soybean Cake under Rapid Pyrolysis.* Energy & Fuels, 2010. **24**(11): p. 6166-6171.
  74. Weiland, N.T., N.C. Means, and B.D. Morreale, *Product distributions from isothermal co-pyrolysis of coal and biomass.* Fuel, 2012. **94**: p. 563-570.
  75. Wang, M., et al., *Interactions between corncob and lignite during temperature-programmed co-pyrolysis.* Fuel, 2015. **142**: p. 102-108.
  76. Mohan, D., C.U. Pittman, and P.H. Steele, *Pyrolysis of Wood/Biomass for Bio-oil: A Critical Review.* Energy & Fuels, 2006. **20**(3): p. 848-889.
  77. Zhu, W., W. Song, and W. Lin, *Catalytic gasification of char from co-pyrolysis of coal and biomass.* Fuel Processing Technology, 2008. **89**(9): p. 890-896.
  78. Ulloa, C.A., A.L. Gordon, and X.A. García, *Thermogravimetric study of interactions in the pyrolysis of blends of coal with radiata pine sawdust.* Fuel Processing Technology, 2009. **90**(4): p. 583-590.
  79. Yangali, P., A.M. Celaya, and J.L. Goldfarb, *Co-pyrolysis reaction rates and activation energies of West Virginia coal and cherry pit blends.* Journal of Analytical and Applied Pyrolysis, 2014. **108**: p. 203-211.
  80. Kastanaki, E., et al., *Thermogravimetric studies of the behavior of lignite–biomass blends during devolatilization.* Fuel Processing Technology, 2002. **77-78**: p. 159-166.
  81. Vamvuka, D., et al., *Pyrolysis characteristics and kinetics of biomass residuals mixtures with lignite* ☆. Fuel, 2003. **82**(15): p. 1949-1960.
  82. Song, Y., A. Tahmasebi, and J. Yu, *Co-pyrolysis of pine sawdust and lignite in a thermogravimetric analyzer and a fixed-bed reactor.* Bioresource Technology, 2014. **174**: p. 204-211.
  83. Fei, J., et al., *Synergistic effects on co-pyrolysis of lignite and high-sulfur swelling coal.* Journal of Analytical and Applied Pyrolysis, 2012. **95**: p. 61-67.
  84. Wan, K., et al., *Experimental and modeling study of pyrolysis of coal, biomass and blended coal–biomass particles.* Fuel, 2015. **139**: p. 356-364.
  85. Yang, X., et al., *Co-pyrolysis of Chinese lignite and biomass in a vacuum reactor.* Bioresource Technology, 2014. **173**: p. 1-5.
  86. Mok, W.S.L. and M.J. Antal, *Effects of pressure on biomass pyrolysis. I. Cellulose pyrolysis products.* Thermochemica Acta, 1983. **68**(2): p. 155-164.
  87. Mao, Y., et al., *Fast co-pyrolysis of biomass and lignite in a micro fluidized bed reactor analyzer.* Bioresource Technology, 2015. **181**: p. 155-162.
  88. Zhang, Y., et al., *Effect of fuel origin on synergy during co-gasification of biomass and coal in CO<sub>2</sub>.* Bioresource Technology, 2016. **200**: p. 789-794.
  89. Collins, S. and P. Ghodke, *Kinetic parameter evaluation of groundnut shell pyrolysis through use of thermogravimetric analysis.* Journal of environmental chemical engineering, 2018. **6**(4): p. 4736-4742.
  90. Ghodke, P. and R.N. Mandapati, *Kinetic modeling of Indian rice husk pyrolysis.* International Journal of Chemical Reactor Engineering, 2018. **16**(2).

91. Mandapati, R.N. and P.K. Ghodke, *Kinetics of pyrolysis of cotton stalk using model-fitting and model-free methods*. Fuel, 2021. **303**: p. 121285.
92. Galwey, A.K. and M.E. Brown, *Kinetic background to thermal analysis and calorimetry*, in *Handbook of thermal analysis and calorimetry*. 1998, Elsevier. p. 147-224.
93. Helsen, L. and E. Van den Bulck, *Kinetics of the low-temperature pyrolysis of chromated copper arsenate-treated wood*. Journal of Analytical and Applied Pyrolysis, 2000. **53**(1): p. 51-79.
94. White, J.E., W.J. Catallo, and B.L. Legendre, *Biomass pyrolysis kinetics: A comparative critical review with relevant agricultural residue case studies*. Journal of Analytical and Applied Pyrolysis, 2011. **91**(1): p. 1-33.
95. Flynn, J.H., *Temperature dependence of the rate of reaction in thermal analysis: the Arrhenius equation in condensed phase kinetics*. Journal of Thermal Analysis and Calorimetry, 1990. **36**(4): p. 1579-1593.
96. Gupta, A., S.K. Thengane, and S. Mahajani, *Kinetics of pyrolysis and gasification of cotton stalk in the central parts of India*. Fuel, 2020. **263**: p. 116752.
97. Ghodke, P. and R.N. Mandapati, *Investigation of particle level kinetic modeling for babul wood pyrolysis*. Fuel, 2019. **236**: p. 1008-1017.
98. Anca-Couce, A., *Reaction mechanisms and multi-scale modelling of lignocellulosic biomass pyrolysis*. Progress in Energy and Combustion Science, 2016. **53**: p. 41-79.
99. Vyazovkin, S., *Modification of the integral isoconversional method to account for variation in the activation energy*. Journal of Computational Chemistry, 2001. **22**(2): p. 178-183.
100. Akahira, T. and T. Sunose, *Method of determining activation deterioration constant of electrical insulating materials*. Res Rep Chiba Inst Technol (Sci Technol), 1971. **16**(1971): p. 22-31.
101. Flynn, J.H. and L.A. Wall, *A quick, direct method for the determination of activation energy from thermogravimetric data*. Journal of Polymer Science Part B: Polymer Letters, 1966. **4**(5): p. 323-328.
102. Hu, Z., et al., *Characteristics and kinetic studies of Hydrilla verticillata pyrolysis via thermogravimetric analysis*. Bioresource technology, 2015. **194**: p. 364-372.
103. Coats, A.W. and J.P. Redfern, *Kinetic parameters from thermogravimetric data*. Nature, 1964. **201**(4914): p. 68-69.
104. Maurya, R., et al., *Non-isothermal pyrolysis of de-oiled microalgal biomass: kinetics and evolved gas analysis*. Bioresource technology, 2016. **221**: p. 251-261.
105. Ma, Z., et al., *Comparison of the thermal degradation behaviors and kinetics of palm oil waste under nitrogen and air atmosphere in TGA-FTIR with a complementary use of model-free and model-fitting approaches*. Journal of Analytical and Applied Pyrolysis, 2018. **134**: p. 12-24.
106. Vyazovkin, S., et al., *ICTAC Kinetics Committee recommendations for performing kinetic computations on thermal analysis data*. Thermochimica acta, 2011. **520**(1-2): p. 1-19.
107. Soria-Verdugo, A., et al., *Comparison of wood pyrolysis kinetic data derived from thermogravimetric experiments by model-fitting and model-free methods*. Energy

- Conversion and Management, 2020. **212**: p. 112818.
108. Li, B., et al., *Study of combustion behaviour and kinetics modelling of Chinese Gongwusu coal gangue: Model-fitting and model-free approaches*. Fuel, 2020. **268**: p. 117284.
  109. Çepeliogullar, Ö., H. Haykırı-Açma, and S. Yaman, *Kinetic modelling of RDF pyrolysis: Model-fitting and model-free approaches*. Waste Management, 2016. **48**: p. 275-284.
  110. Hu, J., et al., *Effectiveness of wind turbine blades waste combined with the sewage sludge for enriched carbon preparation through the co-pyrolysis processes*. Journal of Cleaner Production, 2018. **174**: p. 780-787.
  111. Jayaraman, K., M.V. Kok, and I. Gokalp, *Thermogravimetric and mass spectrometric (TG-MS) analysis and kinetics of coal-biomass blends*. Renewable Energy, 2017. **101**: p. 293-300.
  112. Zakrzewski, R., *Pyrolysis kinetics of wood comparison of iso and polythermal thermogravimetric methods*. Electronic Journal of Polish Agricultural Universities, 2003. **6**(2).
  113. Reina, J., E. Velo, and L. Puigjaner, *Thermogravimetric study of the pyrolysis of waste wood*. Thermochemica acta, 1998. **320**(1-2): p. 161-167.
  114. Nyoni, B., et al., *Co-pyrolysis of South African bituminous coal and Scenedesmus microalgae: Kinetics and synergistic effects study*. International Journal of Coal Science & Technology, 2020. **7**(4): p. 807-815.
  115. Wang, J., et al., *Thermal Behaviors and Kinetics of Pingshuo Coal/Biomass Blends during Copyrolysis and Cocombustion*. Energy & Fuels, 2012. **26**(12): p. 7120-7126.
  116. Florentino-Madiedo, L., et al., *Evaluation of synergy during co-pyrolysis of torrefied sawdust, coal and paraffin. A kinetic and thermodynamic study*. Fuel, 2021. **292**: p. 120305.
  117. Masnadi, M.S., et al., *Fuel characterization and co-pyrolysis kinetics of biomass and fossil fuels*. Fuel, 2014. **117**: p. 1204-1214.
  118. Naqvi, S.R., et al., *Synergistic effect on co-pyrolysis of rice husk and sewage sludge by thermal behavior, kinetics, thermodynamic parameters and artificial neural network*. Waste Management, 2019. **85**: p. 131-140.
  119. Özsin, G. and A.E. Pütün, *Co-pyrolytic behaviors of biomass and polystyrene: Kinetics, thermodynamics and evolved gas analysis*. Korean Journal of Chemical Engineering, 2018. **35**(2): p. 428-437.
  120. Muigai, H.H., et al., *Co-pyrolysis of biomass blends: Characterization, kinetic and thermodynamic analysis*. Biomass and Bioenergy, 2020. **143**: p. 105839.
  121. Turmanova, S.C., et al., *Non-isothermal degradation kinetics of filled with rice husk ash polypropene composites*. Express Polym Lett, 2008. **2**(2): p. 133-146.
  122. Xu, Y. and B. Chen, *Investigation of thermodynamic parameters in the pyrolysis conversion of biomass and manure to biochars using thermogravimetric analysis*. Bioresource technology, 2013. **146**: p. 485-493.
  123. Santos, V.O., et al., *Pyrolysis of acai seed biomass: Kinetics and thermodynamic parameters using thermogravimetric analysis*. Bioresource Technology Reports, 2020. **12**: p. 100553.

124. Zaker, A., et al., *Co-pyrolysis of sewage sludge and low-density polyethylene – A thermogravimetric study of thermo-kinetics and thermodynamic parameters*. Journal of Environmental Chemical Engineering, 2021. **9**(1): p. 104554.

# Chapter 3

## Material and Method

### 3.1 Sample collection and blends preparation

The bituminous coal (100C), sawdust (100SD), and wild hemp (100H) were used to prepare the blends. The C, SD, and H were locally collected from fields and power plants. Figure 3-1 illustrates the schematic diagram of coal-biomass blends preparation. Initially, the samples were dried for 1 day at 105 °C to remove moisture

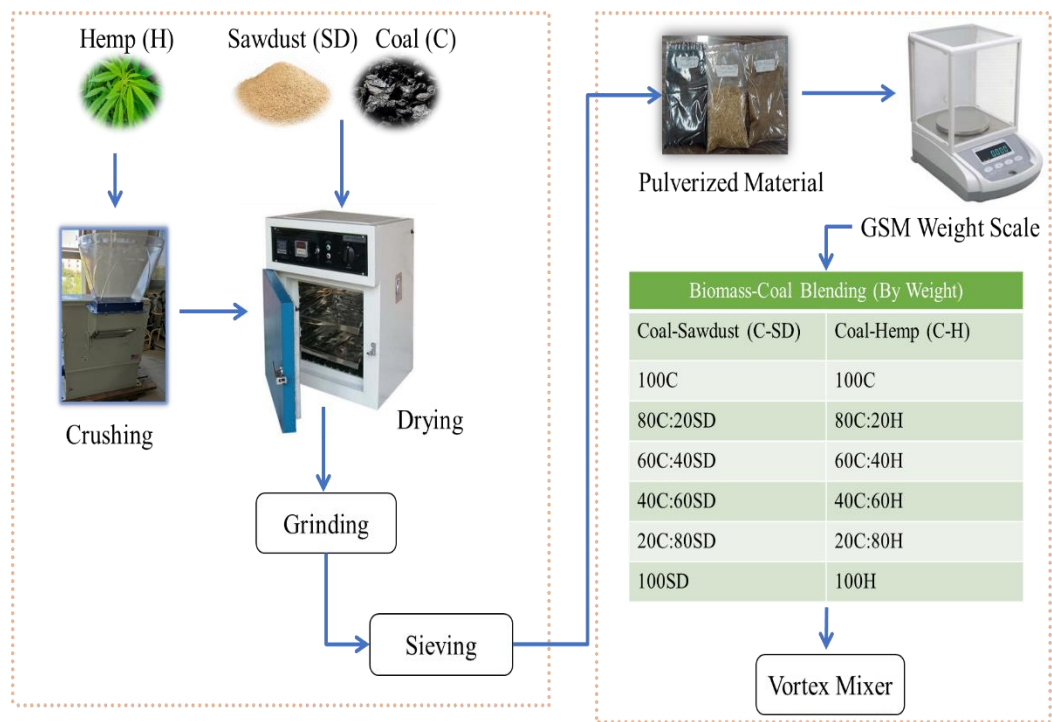


**Figure 3-1** Coal-biomass samples and blends preparation schematic diagram (self-created)

After this, the samples were ground in a Hard Grove Grindability Index Tester (USA) and sieved using Sieving WS Tyler RX-29–10 (USA). The particle size of coal and biomass after sieve was 0.63 mm. Co-pyrolysis behaviour was evaluated using a variety of coal-biomass mixtures. The coal-biomass blends were weighted and blended for 30 minutes in a vortex mixer. The coal-sawdust (C-SD) blends with ratios of 80C:20SD, 60C:40SD, 40C:60SD and 20C:80SD, respectively. While coal-hemp (C-H) blends prepared ratios are 80C:20H, 60C:40H, 40C:60H and 20C:80H, respectively for characterizations.

### **3.2 Samples characterization**

The CHN Analyzer 5ECH2200, CKIC, China, was used to determine the proportion of carbon, hydrogen, and nitrogen in each coal-biomass mix. For each sample, an aluminum sheet was put into a socket and filled with 80 mg of each sample. The He, N, and O<sub>2</sub> gases were used to determine the carbon, hydrogen, and nitrogen concentrations in each coal-biomass mix. The conventional approach was followed to conduct the GCV analysis on coal-biomass blends in a Parr 6200 isoperibol oxygen bomb calorimeter (ASTM D5865-13). For the GCV study, the 0.5 grams of each mix were put into the calorimeter. Agilent Technologies' Cary 630 was used to do FTIR analysis on coal and biomass functional groups (USA). With a scan resolution of 2 cm<sup>-1</sup>, the infrared spectrum's absorption extends from 4000 to 650 centimeters per second. The Diamond ATR module was used for the measurements.

TGA 5500 was used to conduct the TGA of coal-biomass blends, as previously stated (TA Equipments, USA). TGA analysis was performed using a platinum pan on about 10 mg of each sample. An N<sub>2</sub> flow rate of 35 ml min<sup>-1</sup> was used to heat each coal-biomass mix to 25-900 °C for Co-pyrolysis. In this experiment, the heating rate was set at 20°C min<sup>-1</sup>. Each experiment began with a blank test to ensure that there was no systematic fault in the equipment. By forcing the derivative of ML in relation to temperature, the differential thermogravimetric (DTG) was achieved. A set of kinetics and thermodynamic parameters were computed using the TGA data.

### 3.3 Synergistic effect

The additive model was used to find out the synergistic effect in blends of coal-biomass. The additive model compares the experimental values with the calculated values and assumed that there was no interaction observed during co-processing [1]. The calculated values can be estimated using Eq. 3-1

$$Y_{cal} = X_{biomass} \cdot Y_{biomass} + X_{coal} \cdot Y_{coal} \quad \text{Eq. 3-1}$$

Where  $Y_{biomass}$ ,  $Y_{coal}$  are the experimental values obtained from TGA/DTG of individual fuels, while  $X_{biomass}$ ,  $X_{coal}$  is the mass ratio of biomass and coal in the blend, respectively.

The deviation of ML, RL, and  $DTG_{max}$  was determined by Eq. 3-2, which support an evaluation of the presence or absence of synergistic effect during co-pyrolysis [2].

$$Deviation (\%) = \frac{Y_{exp} - Y_{cal}}{Y_{cal}} \times 100 \quad \text{Eq. 3-2}$$

Where  $Y_{exp}$  was the experimental values obtained during TGA/DTG analysis and  $Y_{cal}$  was the calculated values calculated from Eq. 3-1.

### 3.4 Kinetics study

The kinetics of co-pyrolysis is a very complicated process since it involves so many reactions. The Coats-Redfern method was adopted by many researchers to evaluate the kinetics behavior during co-pyrolysis [3]. To calculate the  $E_a$  and  $A$  more precisely, the decomposition of blends was divided into two stages namely as first stage and the second stage [4]. Moisture content stages were not included in the calculation of kinetics parameters. The decomposition of coal-biomass blends can be defined by the rate equation as presented in Eq. 3-3.

$$\frac{d\alpha}{dT} = \beta \cdot k(T) \cdot f(\alpha) \quad \text{Eq. 3-3}$$

Where  $\alpha$  is the conversion factor,  $k$  is the rate constant,  $f(\alpha)$  is the reaction model,  $\beta$  is the heating rate. The conversion factor ( $\alpha$ ) is defined as in Eq. 3-4,

$$\alpha = \frac{w_i - w_t}{w_i - w_f} \quad \text{Eq. 3-4}$$

Where  $w_i$  is the initial weight,  $w_f$  is the final weight, and  $w_t$  is the instantaneous weight of material. The rate constant  $k(T)$  is defined in Eq. 3-5.

$$k(T) = A \exp\left(-\frac{E_a}{RT}\right) \quad \text{Eq. 3-5}$$

Where,  $E_a$  is the activation energy,  $A$  is the pre-exponential factor,  $R$  is the gas constant ( $R=8.314 \text{ J.K}^{-1}.\text{mol}^{-1}$ ), and  $T$  is the absolute temperature in Kelvin.

By putting rate constant from Eq. 3-5 into rate equation Eq. 3-3. The rate equation can be simplified as in Eq. 3-6.

$$\frac{d\alpha}{dT} = \beta \cdot A \exp\left(-\frac{E_a}{RT}\right) \cdot f(\alpha) \quad \text{Eq. 3-6}$$

By taking integral of Eq. 3-6, that gives a straight-line equation Eq. 3-7.

$$\ln \frac{(g(\alpha))}{T^2} = \ln \frac{AR}{\beta E_a} \left(1 - \frac{2RT}{E_a}\right) - \frac{E_a}{RT} \quad \text{Eq. 3-7}$$

Where  $(1-2RT/E_a)$  is assumed to be small and can be neglected from Eq. 3-7. Hence, it can be written as presented in Eq. 3-8.

$$\ln \frac{(g(\alpha))}{T^2} = \ln \frac{AR}{\beta E_a} - \frac{E_a}{RT} \quad \text{Eq. 3-8}$$

Coats-Redfern is a model-fitting method, and it approaches the most suitable integral function  $(g(\alpha))$  to determine the decomposition kinetics of solid substance. The most frequent  $g(\alpha)$  is implemented from the literature [5] are provided in Table 3-1.

**Table 3-1** Algebraic expressions for reaction mechanism  $g(\alpha)$  for solid state reaction

Symbols	Functions	$g(\alpha)$
Power law for acceleratory reaction mechanism ( )		
R1	Contracting-disk	$\alpha$
Phase boundary for deceleratory reaction mechanism		
R2	Contracting-cylinder	$1 - (1 - \alpha)^{1/2}$
R3	Contracting-sphere	$1 - (1 - \alpha)^{1/3}$
Diffusion mechanism		
D1	Parabolic-law	$\alpha^2$
D2	Valansi-equation	$\alpha + (1 - \alpha) \ln (1 - \alpha)$
D3	Jander-equation	$[(1 - (1 - \alpha)^{1/3})^2]$
D4	G. Brounstein-equation	$1 - 2\alpha/3 - (1 - \alpha)^{2/3}$
Mechanism non-invoking equations or chemical process		
F1/3	One and third order	$-3/2[1 - (1 - \alpha)^{2/3}]$

F1	First order	$-\ln(1 - \alpha)$
F3/2	One and a half order	$2[(1 - \alpha)^{-1/2} - 1]$
F2	Second order	$(1 - \alpha)^{-1} - 1$
F3	Third order	$1/2[(1 - \alpha)^{-2} - 1]$
F4	Forth order	$1/3[(1 - \alpha)^{-3} - 1]$

To evaluate the kinetic parameter during co-pyrolysis, the Coats-Redfern method with thirteen  $g(\alpha)$  was implemented. Arrhenius plot for thirteen  $g(\alpha)$  was plotted between  $\ln[g(\alpha)/T^2]$  vs  $1/T$  which gives a straight line. Additionally, if precise  $g(\alpha)$  is implement, the plot gives a straight line having high value of linear regression ( $R^2$ ) from which the value of  $E_a$  and  $A$  could be derived. The  $E_a$  can be calculated from the slope of the line,  $-E_a/R$ , and the intercept of the line is directly used to calculate the  $A$ . The  $g(\alpha)$  describes the mechanism that controls the reaction, the shape, and the size of the reacting particles. The  $g(\alpha)$  with the highest  $R^2$  will be considered as the function of the model that best describes the reaction kinetics of ML at a specific stage.

### 3.5 Thermodynamics parameters

Thermodynamic parameters were calculated after selecting the most suitable  $g(\alpha)$  and using kinetics parameters ( $E_a$  and  $A$ ) of that  $g(\alpha)$ . The change in enthalpy ( $\Delta H$ ) and change in Gibbs free energy ( $\Delta G$ ) were calculated through Eq. 3-9 and Eq. 3-10, respectively. The change in entropy ( $\Delta S$ ) was calculated from Eq. 3-11. These equations were taken from the literature [6].

$$\Delta H = E_a - RT_p \quad \text{Eq. 3-9}$$

$$\Delta G = E_a + RT_p \ln (K_b T_p / hA) \quad \text{Eq. 3-10}$$

$$\Delta S = (\Delta H - \Delta G) / T_p \quad \text{Eq. 3-11}$$

Where  $T_p$ ,  $h$ ,  $K_b$ , and  $R$  is the peak decomposition temperature, Plank's constant ( $6.626 \times 10^{-34}$  J.s), Boltzmann constant ( $1.381 \times 10^{-23}$  J/K), and gas constant, respectively.

### 3.6 Experimental setup for the bio-char formation

To evaluate the further feasibility of hemp biomass for energy purposes, the bio-char of hemp was prepared by pyrolysis. Figure 3-2 illustrates the schematic diagram for the formation of bio-char from hemp. The N<sub>2</sub> gas was feed with a flowrate of 40 ml min<sup>-1</sup> for pyrolysis of hemp via a fixed bed reactor (FBR). The FBR contained a cylindrical stainless-steel tube (SS-316) and had 14 mm outer and 12 mm inner diameter, while the length of the tube was 40 cm. The sample was placed in the middle of the tube and the tube was held with quartz wool by both ends. The electric heater externally heats the furnace and a thermocouple was placed near the sample bed to monitor the temperature. The 10 g of sample was fed into the sample bed. The set temperature was 520 °C with 10 °C/min of heating rate. The yield% of bio-char was calculated by Eq. 3-12 [7].

$$\% \text{ Yield of biochar} = \frac{\text{wt. of biochar produced}}{\text{wt. of biomass sample}} \times 100 \quad \text{Eq. 3-12}$$

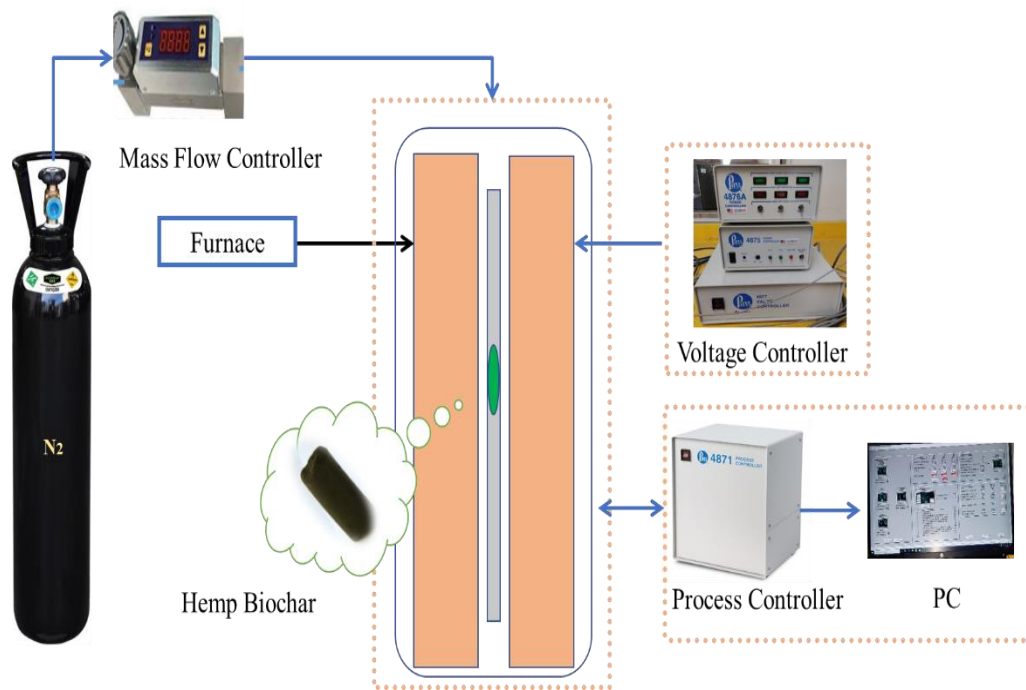


**Figure 3-2** Hemp bio-char production via fixed bed reactor schematic diagram (self-created)

### 3.6.1 Bio-char characterization

The FTIR analysis was done to evaluate the functional groups present in hemp bio-char, while the TGA was performed to observe the ML and RL of bio-char. The conditions for FTIR and TGA analysis of bio-char were the same as coal-biomass blends that are mentioned in the above sections. The surface morphology and elemental composition of hemp bio-char were examined by an SEM-EDX analyzer (JSM-6490A of JEOL, Japan) combined with an X-ray energy dispersive (EDX) analyzer.

## Summary

The coal (bituminous coal) and biomass (sawdust, hemp) were collected locally and prepared according to the literature. The materials were dried in oven for 24 h at 105 °C to remove moisture content. Both coal and biomass had a particle sizes of 0.63 mm after sieving. The blends were prepared at 20,40,60,80 % of biomass in the blend. The CHN analysis was performed to evaluate carbon, hydrogen, and nitrogen content in blends. The GCV analysis of blends were performed in oxygen bomb calorimeter. The GCV analysis investigate the calorific value variation with the addition of both coal and biomass in the blend. The FTIR analysis indicated the presence and intensity of different functional group in coal and biomass. With a scan resolution of 2 cm<sup>-1</sup>, the infrared spectrum's absorption extends from 4000 to 650 centimeters per second. Co-pyrolysis was performed in TGA. TGA analysis was performed using a platinum pan on about 10 mg of each sample. An N<sub>2</sub> flow rate of 35 ml min<sup>-1</sup> was used to heat each coal-biomass mix to 25-900 °C for Co-pyrolysis. In this experiment, the heating rate was set at 20°C min<sup>-1</sup>. The synergistic effects in coal-biomass blends were calculated through additive model that observed the presence and intensity of synergistic effect. The Coats Redfern method was implemented to calculate the activation energy and pre-exponential factor of coal-biomass blends. The reaction mechanism for thermal degradation was obtained by comparing results of thirteen integral function. The validity of model depends on the value of linear regression (R<sup>2</sup>). The model that gives the higher value of R<sup>2</sup> (0.9-1), considered as a best model that will describe the thermal degradation mechanism of blends. The thermodynamic parameters were calculated by using best fitted data from kinetics. The kinetics and thermodynamics parameters are helpful in modeling and scaling of co-pyrolysis reactor. To assess the additional viability of hemp biomass for energy purposes, the bio-char of hemp was prepared in fixed bed reactor. The 10 g of hemp fed into the reactor. The set temperature was 520 °C with 10 °C/min of heating rate. The residence time was 2 hr. After bio-char preparation, the bio-char was characterized through FTIR, TGA, and SEM-EDX to investigate its functional groups, thermal stability, and structural morphology.

## References

1. Chen, X., et al., *Thermogravimetric analysis and kinetics of the co-pyrolysis of coal blends with corn stalks*. *Thermochimica Acta*, 2018. **659**: p. 59-65.
2. Merdun, H., Z.B. Laouge, and A.S. Çiğgin, *Synergistic effects on co-pyrolysis and co-combustion of sludge and coal investigated by thermogravimetric analysis*. *Journal of Thermal Analysis and Calorimetry*, 2021.
3. Naqvi, S.R., et al., *Pyrolysis of high ash sewage sludge: Kinetics and thermodynamic analysis using Coats-Redfern method*. *Renewable Energy*, 2019. **131**: p. 854-860.
4. Liu, X., M. Chen, and Y. Wei, *Kinetics based on two-stage scheme for co-combustion of herbaceous biomass and bituminous coal*. *Fuel*, 2015. **143**: p. 577-585.
5. Naqvi, S.R., et al., *Synergistic effect on co-pyrolysis of rice husk and sewage sludge by thermal behavior, kinetics, thermodynamic parameters and artificial neural network*. *Waste Management*, 2019. **85**: p. 131-140.
6. Ding, G., et al., *Synergistic effect, kinetic and thermodynamics parameters analyses of co-gasification of municipal solid waste and bituminous coal with CO<sub>2</sub>*. *Waste Management*, 2021. **119**: p. 342-355.
7. Ma, Z., et al., *In-depth comparison of the physicochemical characteristics of bio-char derived from biomass pseudo components: Hemicellulose, cellulose, and lignin*. *Journal of Analytical and Applied Pyrolysis*, 2019. **140**: p. 195-204.

# Chapter 4

## Results and Discussion

### 4.1 Materials Characterization

The CHN analysis of coal-biomass blends is presented in Table 4-1. The 100C was contained the high content of carbon (67%) as compared to 100SD (47%) and 100H (44%). Biomass has a lower percentage of carbon content while having high moisture, oxygen, hydrogen content [1]. The carbon content of blends decreased by increasing the biomass ratio that is due to the reduction effect of low carbon content in biomass [2]. The compositions of both biomasses are different because each biomass has unique formation conditions and origins that can cause to increase or decrease various elements and phases [3]. Therefore, when comparing the carbon content of both biomasses, 100SD contained slightly high carbon content than 100H. Consequently, the blends of C-SD have a higher value of carbon content (53-64%) as compared to C-H blends (49-64%). A higher char yield is obtained if the fuel contains a high amount of carbon content [4].

The hydrogen content of 100C was lower (3.55%) than 100SD (7.17%) and 100H (6.94%), respectively. The blends of C-SD have slightly higher hydrogen content as compared to C-H blends. The H/C atomic ratio defines the energy content of any fuel as the process in an inert environment as the reaction retains a high H/C ratio by reducing the formation of H<sub>2</sub>O and CO<sub>2</sub>, hence resulting in higher energy content [5]. The H/C ratio of 100C was 0.05 which is far less than 100SD (0.15) and 100H (0.15). Generally, biomass has a high H/C ratio as compared to coal, so biomass provides more hydrogen resources to play a dominant role in hydrogenation [6]. Nitrogen content in fuel causes to produce NO<sub>x</sub> emission. It could be seen that nitrogen content in 100C (0.47%) was slightly higher than that of 100SD (0.09%), while 100H (2.8%) contained higher nitrogen content than 100C. The CHN of 100H is related with literature observation [7].

**Table 4-1** Ultimate analysis (CHN) of coal-biomass blends

Sample	Carbon%	Hydrogen%	H/C	Nitrogen%
100C	67	3.55	0.05	0.47
80C:20SD	64	4.00	0.06	0.28
60C:40SD	61	4.90	0.08	0.23
40C:60SD	56	5.13	0.09	0.21
20C:80SD	53	6.16	0.11	0.23
100SD	47	7.17	0.15	0.09
80C:20H	64	3.9	0.06	0.81
60C:40H	59	4.32	0.07	1.26
40C:60H	52	4.47	0.08	1.71
20C:80H	49	5.39	0.11	2.12
100H	44	6.94	0.15	2.8

The GCV of coal-biomass blends is compiled in Figure 4-1. The 100C shows the highest GCV (29.6 MJ/kg) as compared to 100SD (20.5 MJ/kg) and 100H (18 MJ/kg). Figure 4-1 (a) shows the GCV analysis of C-SD blends. The highest and lowest GCV is observed for 80C:20SD (29 MJ/kg) and 20C:80SD (23.7 MJ/kg), respectively which is higher than 100SD because coal blend with biomass increases the GCV of coal-biomass blend [8]. Therefore, the blending of coal with biomass increases the GCV of biomasses. Figure 4-1 (b) illustrates the GCV analysis of C-H blends. It could be seen that the highest GCV is for 80C:20H (29 MJ/kg), while the lowest GCV is for 20C:80H (21.7 MJ/kg). The GCV of 100SD was greater than 100H. Furthermore, it is also observed that the 80C:20SD and 80C:20H blends have the same GCV (29 MJ/kg) that may be due to the same percentage of carbon content (64%) in both blends as previously investigated in the CHN analysis. The main component of biomass fuels is carbon, hydrogen, and oxygen,

while carbon and hydrogen content influences the GCV of the fuel during combustion by exothermic reaction [4].

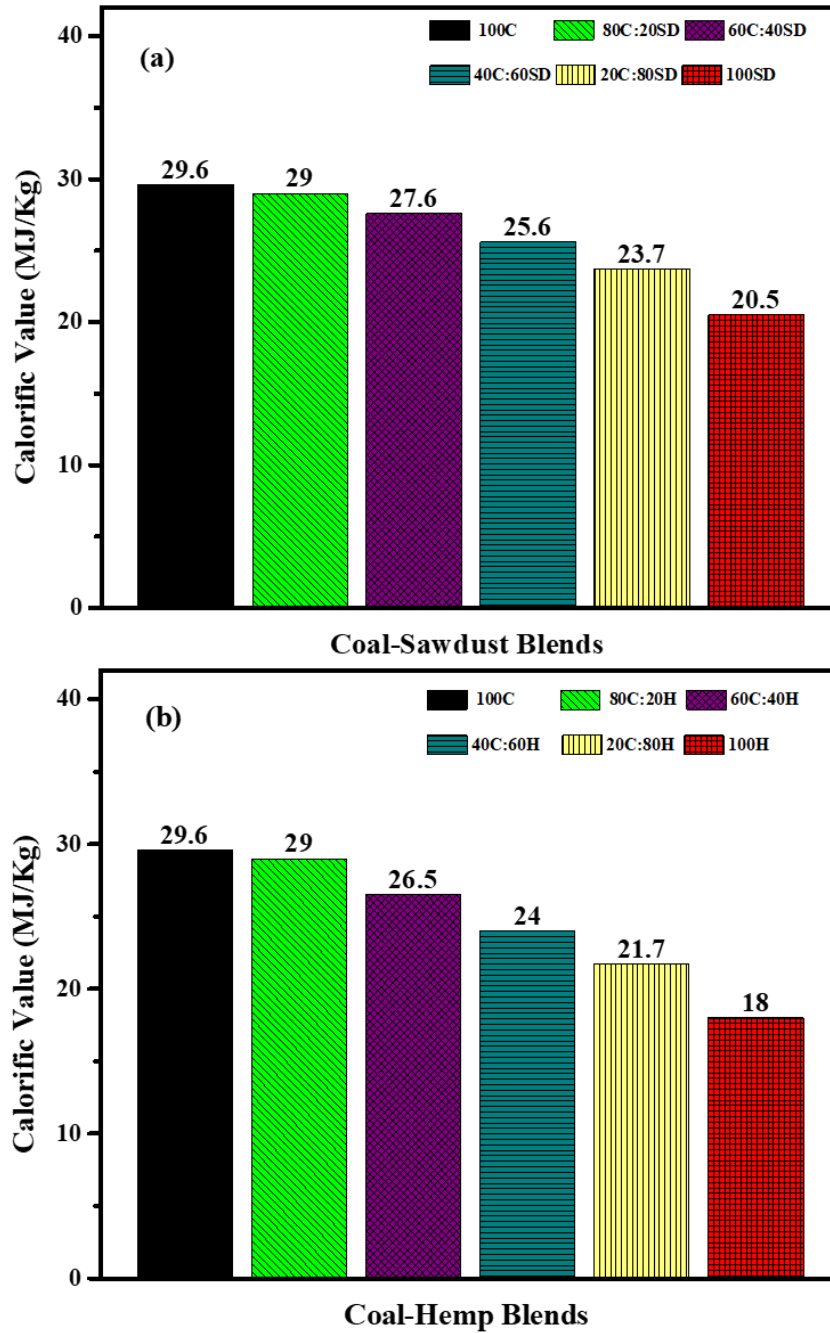
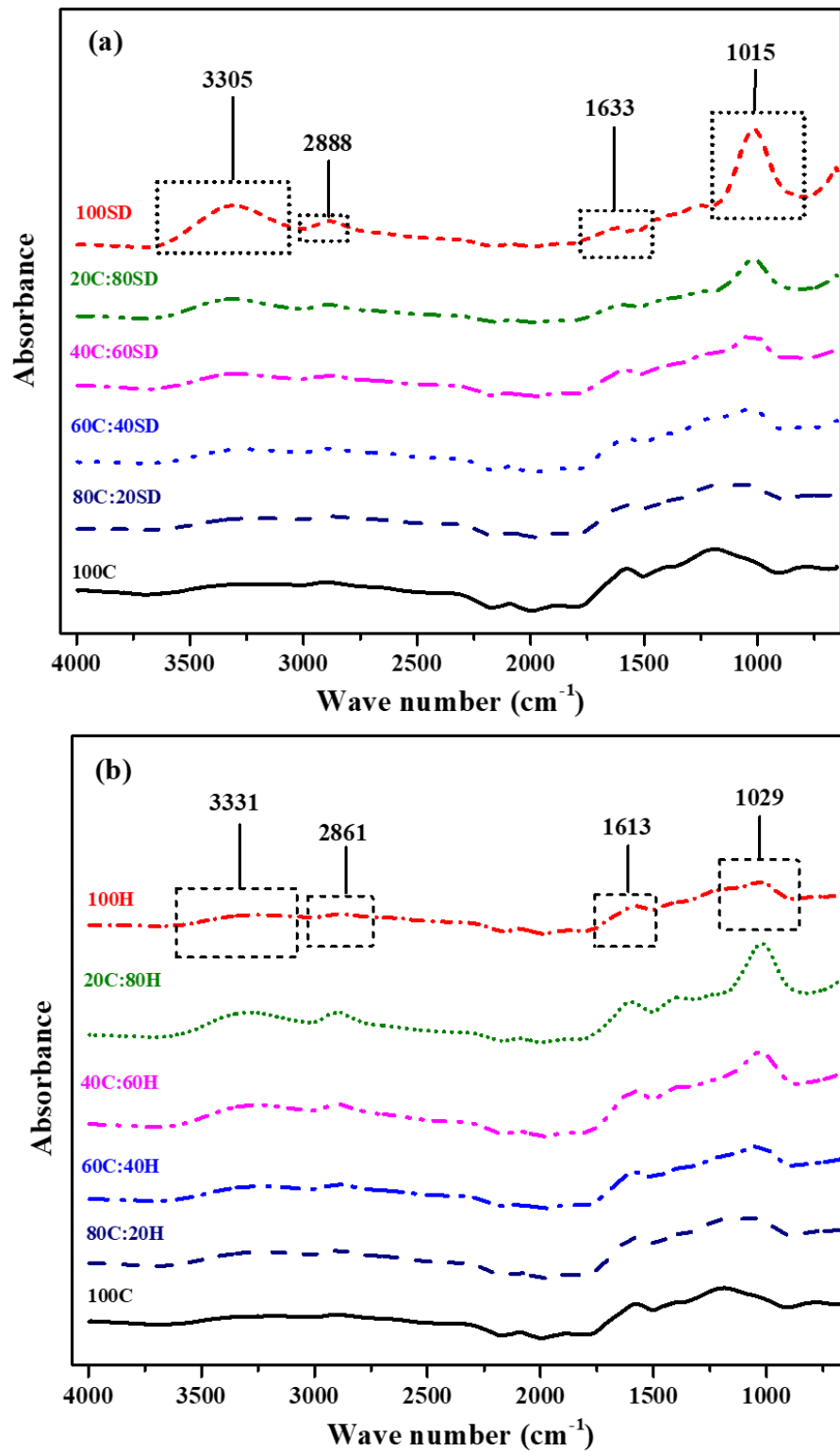


Figure 4-1 GCV measurement of coal-biomass blends (a) C-SD (b) C-H

Figure 4-2 (a) illustrates the FTIR spectra of C-SD blends. It could be seen that there is a considerable difference in functional groups of 100C and 100SD main functional groups. There are two major absorption ranges in 100C. The first absorption peak in 100C was appeared at 1640-1500  $\text{cm}^{-1}$  that is attributing the stretching vibration of C=C aromatic ring [9] whereas the second absorption peak is detected in the range of 2990-2800  $\text{cm}^{-1}$  that indicating the presence of the methylene group in saturated aliphatic C-H [10]. The weak peak around 3420-3510  $\text{cm}^{-1}$  was due to the of OH group like alcoholic or phenolic compounds present in 100C [11]. Additionally, the C=O at 1770-1640  $\text{cm}^{-1}$  and the C-O at 1320-1130  $\text{cm}^{-1}$  stretching vibration seem to be very weak in 100C. In 100SD, noticeable stretching and broadening peak at 3305  $\text{cm}^{-1}$  is indicating the hydroxyl stretching (O-H). The O-H group is abundantly found in all biomasses as compared to coal. It reveals that the biomass macromolecular network contains a higher percentage of hydrogen than coal as Table 4-1 illustrated. Dai et al. [12] reported nearly the same peak for C-O stretching vibration for cellulose and hemicellulose.

The FTIR spectra of C-H blends are shown in Figure 4-2 (b). A noticeable stretching peak at 3331  $\text{cm}^{-1}$  for 100H is attributed to O-H stretching. Rajinipriya et al. [13] reported the same absorption peak in this range for hemp at 3400  $\text{cm}^{-1}$  which is due to the hydroxyl group or O-H stretching. The peak observed at 2861  $\text{cm}^{-1}$  was due to the aliphatic stretching vibration of C-H group. Moonart et al. [14] also observed the same peak in this range for aliphatic C-H stretching vibration in cellulose and hemicellulose. Additionally, another two weak peaks of 1613  $\text{cm}^{-1}$  and 1029  $\text{cm}^{-1}$  are observed in Figure 4-2 (b) for 100H is due to aromatic C=C stretching vibrations [13] and C-O stretching vibration [15], respectively. Additionally, it could be seen that 100SD and 100H biomass have almost the same functional groups, but the absorption intensity or percentage of relative contents are different. Therefore, when coal blended with biomass, the intensity of functional groups changed. The coal-biomass blends showed the intermediate behavior in terms of band intensity and percentage of relative content present in both coal and biomass.



**Figure 4-2** FTIR analysis of coal-biomass blends (a) C-SD (b) C-H

The absorption intensity of 100SD for the O-H bond was highest as compared to 100C and 100H that is indicating higher content of hydrogen present in 100SD as shown previously in the CHN analysis. The C=C aromatic ring stretching vibrations intensity of 100SD was also observed high than 100H. However, 100SD has less C=C aromatic ring stretching than 100C is indicating that the 100SD has low carbon content than 100C and high carbon content than 100H. For coal-biomass blends, the band intensity of O-H stretching reduced and the intensity of aromatic ring C=C increases. This situation may be due to the reduction of oxygen and hydrogen content from biomass by blending it with coal that may causes to increase the carbon content in blends. Hence, increases the GCV of coal-biomass blends by increasing its carbon content percentage.

Figure 4-3 demonstrates the TGA and DTG pyrolysis profile of coal-biomass blends. It could be seen that individual fuels and their blends are illustrated ML in three stages: moisture loss, active pyrolysis, and passive pyrolysis Co-pyrolysis investigation of coal-biomass blends are presented in

Table 4-2. The first stage ML of each sample attributes to degradation of low molecular weight component and loss of moisture content. The structural component of biomass such as hemicellulose, cellulose, and lignin. Also, the oxygen-containing species and OH functional groups that fascinate moisture through H-bonding [16]. Figure 4-3 (a-b) represents the TGA and DTG of C-SD blends that show 100SD evolved its moisture content around 30-120 °C, whereas the 100C contained less amount of moisture content than 100SD that evolved during 50-105 °C temperature range. The 100H evolved its moisture content around 30-150 °C temperature range as illustrated in Figure 4-3 (c-d). Mostly, the influence of the moisture content stage was not being considered during the evaluation of kinetics and thermodynamics parameters.

The second stage of individual biomass was representing the active pyrolysis zone. Most of the pyrolysis vapour generates in this stage. Generally, in biomass, the shoulder at a lower temperature in the DTG curve represents the hemicellulose component decomposition, whereas the higher tmeperature range peak corresponds to the cellulose decomposition. The lignin degradation arises in a wider temperature zone [17].

Table 4-2 represents that the major decomposition of individual fuels was started around 365 °C for 100C, 200 °C for 100SD, and 147 °C for 100H. From Figure 4-3 (a-d), it is observed that the devolatilization of 100SD and 100H started earlier than 100C due to the macromolecular structure of biomass that is mainly composed of cellulose, hemicellulose, and lignin which are linked together by ether bond (R-O-R) [18]. However, the structure of coal is composed of polycyclic aromatic hydrocarbons and their thermal stability is much higher than ether bond [19]. Therefore, 100SD and 100H biomass were started to decompose at a low temperature than 100C which decomposed at higher temperature. For individual biomasses, the DTG curve showed that the maximum weight loss occurs at peak decomposition temperature ( $T_p$ ), 376 °C for 100SD and 340 °C for 100H. The  $T_p$  of 100C was observed at 466 °C which is greater than both biomasses.

The volatile matter content in biomass was higher than that of 100C, therefore the  $DTG_{max}$  of 100SD and 100H was higher than 100C. The ML of biomass was also greater than that of 100C as shown in Figure 4-3 (a, c). The third stage, in 100C, and biomasses represent the passive pyrolysis zone, which is due to the biochar formation and decomposition of lignin [20]. The passive pyrolysis zone occurred in a wider temperature range and no peak was observed in this stage due to very slow ML. The RL at the end of the reaction was 65% for 100C, 39% for 100SD, and 47% for 100H. Coal-biomass blends also showed three stages for major decomposition, the first stage was due to moisture evaporation, and it was not significantly changed due to blending, the second stage reflected the biomass ratio in the blend, and the third stage represented the portion of coal in the blend.

Table 4-2, represents the major decomposition zone for coal-biomass and their blends. It could be seen that the coal-biomass blends showed some similar properties to those of individual fuels. Figure 4-3 (b, d) illustrates that the ignition temperature ( $T_i$ ) of 80C-20SD and 80C-20H was lower than 100C and higher than that of individual biomasses.

The lower value of  $T_i$  in co-pyrolysis represents the better activity of blends [20]. The  $T_p$  of 80C-20SD blend during the second and third stages were 383 °C and 449 °C,

respectively. The ML during the second and third stages for the 80C-20SD blend were 15% and 21% respectively. The RL for 80C-20SD was 85% in the second and 59% in the third stage. However, for 80C-20H the  $T_p$  was 339 °C in the second and 479 °C in the third stage, whereas the ML was 14% and 20% during the second and third stage of decomposition, respectively. The RL in second stage for 80C-20H was 83% and in third stage it was 63%. The  $T_p$  of all coal-biomass blends was decreased during the second stage as the ratio of biomass increased in the blends, whereas the  $T_p$  in the third stage increased by increasing the coal ratio. The  $DTG_{max}$  increased with increasing the ratio of biomass in the blend. Additionally, the  $DTG_{max}$  of blends was higher than 100C and less than individual biomass. The ML of blends were in between the individual fuels for each stage as shown in

Table 4-2. In pyrolysis, the OH and H radicals evolved from biomass, increasing the aromatic rings cracking in coal. The 100H and 100SD biomass contained a high hydrogen content as compared to 100C. Therefore, co-pyrolysis of blends generates complex hydrocarbon molecules and their thermal degradation needs more energy [21]. Coal and biomass have different structural properties therefore different pyrolysis behavior was observed. The C-H blends showed a higher RL as compared to C-SD blends, which that represents the C-H blends are suitable in the production of bio-char. Whereas, the ML in C-SD blends are higher than that of C-H blends, which indicates that C-SD blends are suitable in the production of bio-oil.

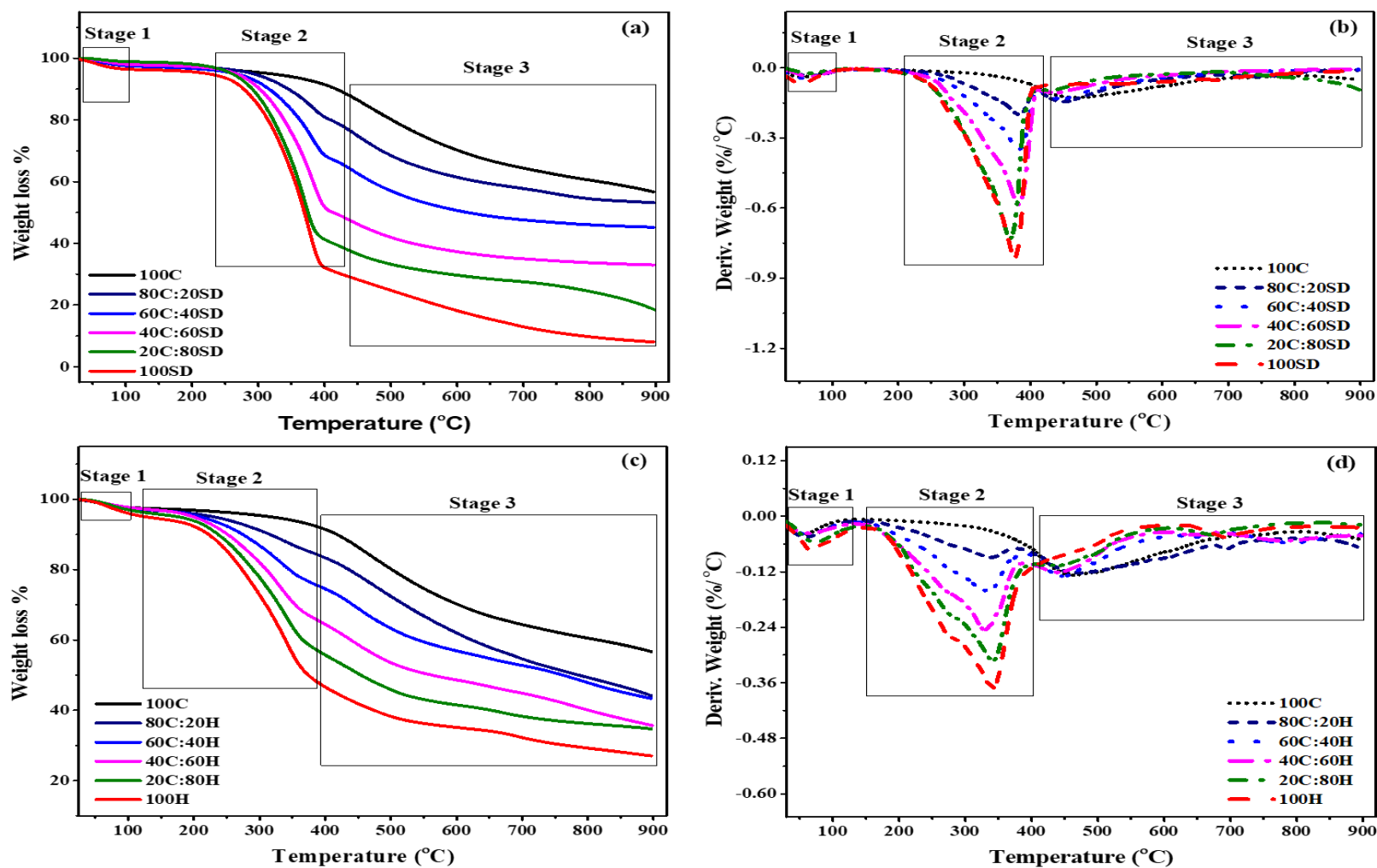


Figure 4-3 TGA/DTG of coal-biomass blends (a) C-SD TGA (b) C-SD DTG (c) C-H TGA (d) C-H DTG

**Table 4-2** Major portions of decomposition of coal-biomass and their blends during pyrolysis in N<sub>2</sub> environment

The second stage (major decomposition zone)						Third stage (major decomposition zone)				
Sample	Temp range °C	T <sub>p</sub> (°C)	ML %	RL %	DTG <sub>max</sub> (%/°C)	Temp range °C	T <sub>p</sub> (°C)	ML %	RL %	DTG <sub>max</sub> (%/°C)
100C	-	-	-	-	-	308-668	466	26	65	-0.130
80C:20SD	250-408	383	15	85	-0.198	408-641	449	21	59	-0.143
60C:40SD	232-410	381	30	70	-0.349	410-605	447	15	51	-0.133
40C:60SD	211-410	381	47	53	-0.584	410-553	438	11	39	-0.109
20C:80SD	200-402	366	57	42	-0.732	402-527	434	9	32	-0.095
100SD	200-401	376	61	39	-0.805	-	-	-	-	-
80C:20H	188-395	339	14	83	-0.088	395-592	479	20	63	-0.123
60C:40H	174-395	332	22	75	-0.162	395-575	447	17	58	-0.129
40C:60H	169-395	331	32	66	-0.248	395-530	445	14	52	-0.121
20C:80H	147-395	341	39	57	-0.311	395-504	442	12	45	-0.108
100H	147-395	340	47	47	-0.370	-	-	-	-	-

## 4.2 Synergistic effect

Table 4-3 presents the synergistic effects observed during co-pyrolysis. For C-SD blend, the deviation of ML was only positive for 20C:80SD (0.024%), while the RL was positive for all C-SD blends. The deviation of DTG<sub>max</sub> for C-SD blends were positive for 40C:60SD (0.091%) and 20C:80SD (0.092%), respectively. In C-H blends, the deviation of ML was positive for all blends except 20C:80H (-0.011%), while the deviation of RL was only positive for 20C:80H (0.056%). The deviation in DTG<sub>max</sub> was negative for all C-H blends.

The positive value for deviation for ML and DTG<sub>max</sub> during bio-char formation indicates the presence of synergistic effect whereas the negative values represent the absence of synergistic effect [22]. The synergistic effect in co-pyrolysis was indicating the interaction of evolved products from biomass and coal [23]. The synergistic effect present in coal-biomass blends may be enlightened by the hydrogen donors and radical exchanges. The biomass and coal have altered H/C ratios, as biomass possesses higher hydrogen content than coal and the hydrogen donor/ acceptor mechanism may affect the coal-biomass co-pyrolysis mechanism [24].

From the above analysis, it is observed that the synergistic effect is mostly present in C-H blends rather than C-SD blends in term of ML that indicating the C-H blends which shows more synergistic effect during co-pyrolysis. Additionally, from C-SD blends the 20C:80SD shows somehow positive synergy, while for C-H blends the 80C:20H, 60C:40H, and 40C:60H show a positive synergistic effect in terms of ML.

**Table 4-3** Synergistic effect calculation in co-pyrolysis of coal-biomass blends

Sample	Experimental			Calculated			Deviation		
	ML%	RL %	DTG <sub>max</sub>	ML%	RL %	DTG <sub>max</sub>	ML%	RL %	DTG <sub>max</sub>
100C	38.85	56.42	0.130	-	-	-	-	-	-
80C:20SD	43.18	53.24	0.198	48.55	46.73	0.265	-0.110	0.139	-0.252
60C:40SD	51.45	45.21	0.349	58.26	37.05	0.400	-0.134	0.220	-0.127
40C:60SD	64.14	33.04	0.584	67.96	27.37	0.535	-0.056	0.207	0.091
20C:80SD	79.59	18.51	0.732	77.67	17.69	0.670	0.024	0.046	0.092
100SD	87.38	8.01	0.805	-	-	-	-	-	-
80C:20H	52.22	44.12	0.088	44.56	50.53	0.178	0.171	-0.126	-0.485
60C:40H	53.18	43.28	0.162	50.27	44.64	0.226	0.057	-0.030	-0.283
40C:60H	60.74	35.72	0.248	55.98	38.75	0.274	0.085	-0.078	-0.094
20C:80H	61.00	34.72	0.311	61.69	32.86	0.322	-0.011	0.056	-0.034
100H	67.41	26.98	0.370	-	-	-	-	-	-

### 4.3 Kinetics Study

The kinetics parameters such as  $E_a$  and  $A$  of coal-biomass blends were calculated by using the TGA. Figure 4-4 shows the  $E_a$  of thirteen solid-state  $g(\alpha)$ . The  $g(\alpha)$  was established to determine the most suitable reaction mechanism by the Coats-Redfern method. The Coats-Redfern model requires only a single heating rate. The kinetic parameters were calculated by presuming a single reaction for a specific stage. As discussed in DTG analysis, there was only a single reaction for individual coal and biomasses during pyrolysis. However, the coal-biomass blends show two reactions for devolatilization. Therefore, Eq. 3-8 was applied to each stage separately and calculated the kinetic parameters of each reaction. Each  $g(\alpha)$  from Table 3-1 gives the straight line with  $R^2$ . The  $g(\alpha)$  having the highest value of  $R^2$  is considered as the best integral function that describes the kinetics of reaction for each stage [25]. The temperature ranges for the kinetics calculation of individual fuels and their blends were taken from

Table 4-2. All models from Table 3-1 show the value of  $R^2$  in the range of 0.90-1 except R1 and F1/3 model in the second stage for 40C:60SD, 20C:80SD, and 20C:80H blends. Figure 4-4 illustrates that the models R1 and F1/3 show negative value in the second stage for 60% and 80% ratio of biomasses which means these models are not suitable for these blends. The highest  $E_a$  for C-SD blend and C-H blends in the first stage were found by the D3 model, while in the second stage F4 model showed the highest value of  $E_a$ .

The R1 model showed the lowest value of  $E_a$  for C-SD blends and C-H blends during the first and second stages. Based on the highest  $R^2$ , Table 4-4 listed the best-fitted  $g(\alpha)$ ,  $E_a$ ,  $R^2$ , and  $A$  for the first and second stages of coal-biomass blends. The first and second stage  $E_a$  for C-SD blends is presented in Figure 4-4 (a-b). For the first stage of the C-SD blend, the R3 model shows the highest value of  $R^2$ , whereas in the second stage the model F3/2 showed the higher value of  $R^2$ . Figure 4-4 (c-d) represents the  $E_a$  for the first and second stages for C-H blends. For the first stage of C-H blends, the F2 model was suitable and for the second stage F1 and F3/2 models showed the highest value of  $R^2$ . The  $E_a$  for 100C was 39 kJ/mol through the F3/2 model, while 100SD and 100H show 60 kJ/mol

through the R3 model, and 44 kJ/mol through the F2 model, respectively. The  $E_a$  for C-SD blends were 43-59 kJ/mol for first stage and 12-31 kJ/mol for second stage. In contrast, the C-H blends showed  $E_a$  of 29-42 kJ/mol in the first stage and 9-26 kJ/mol in the second stage as presented in Table 4-4.

The  $E_a$  for coal-biomass blend in the first stage increased as the ratio of biomass increased, whereas in the second stage the  $E_a$  decreased as the percentage of biomass increased in coal-biomass blends. Tian. et. al [26] also reported that under 350 °C temperature the  $E_a$  of coal-biomass blends increased as biomass ratio in blend increased. The overall minimum  $E_a$  was observed for 20C-80SD (70 kJ/mol) and 20C-80H (51 kJ/mol) during the first and second stages. The  $R^2$  for all coal-biomass blends was in the range of 0.99-1, which confirmed the validity and suitability of the applied model [27].

Generally, the A is related to the material structure, and indicates the collision of molecules in the direction essential to initiate a reaction [28]. The A value calculated for 100C was 53min<sup>-1</sup>, for 100SD was 6208 min<sup>-1</sup>, and for 100H was 1731 min<sup>-1</sup>. As larger the value of A, the more energy is transferred by the collision of the molecules [29]. For C-SD blends the value of A was 77-4290 min<sup>-1</sup> in the first stage and 1.25-22 min<sup>-1</sup> in the second stage. While for C-H blends the value of A during the first and second stage was in the range of 15.90-1053 min<sup>-1</sup> and 0.24-6.38 min<sup>-1</sup>, respectively. The value of A increased in the first stage as the ratio of biomass increased in the coal-biomass blend whereas in the second stage the value of A decreased as the biomass increased in the blend.

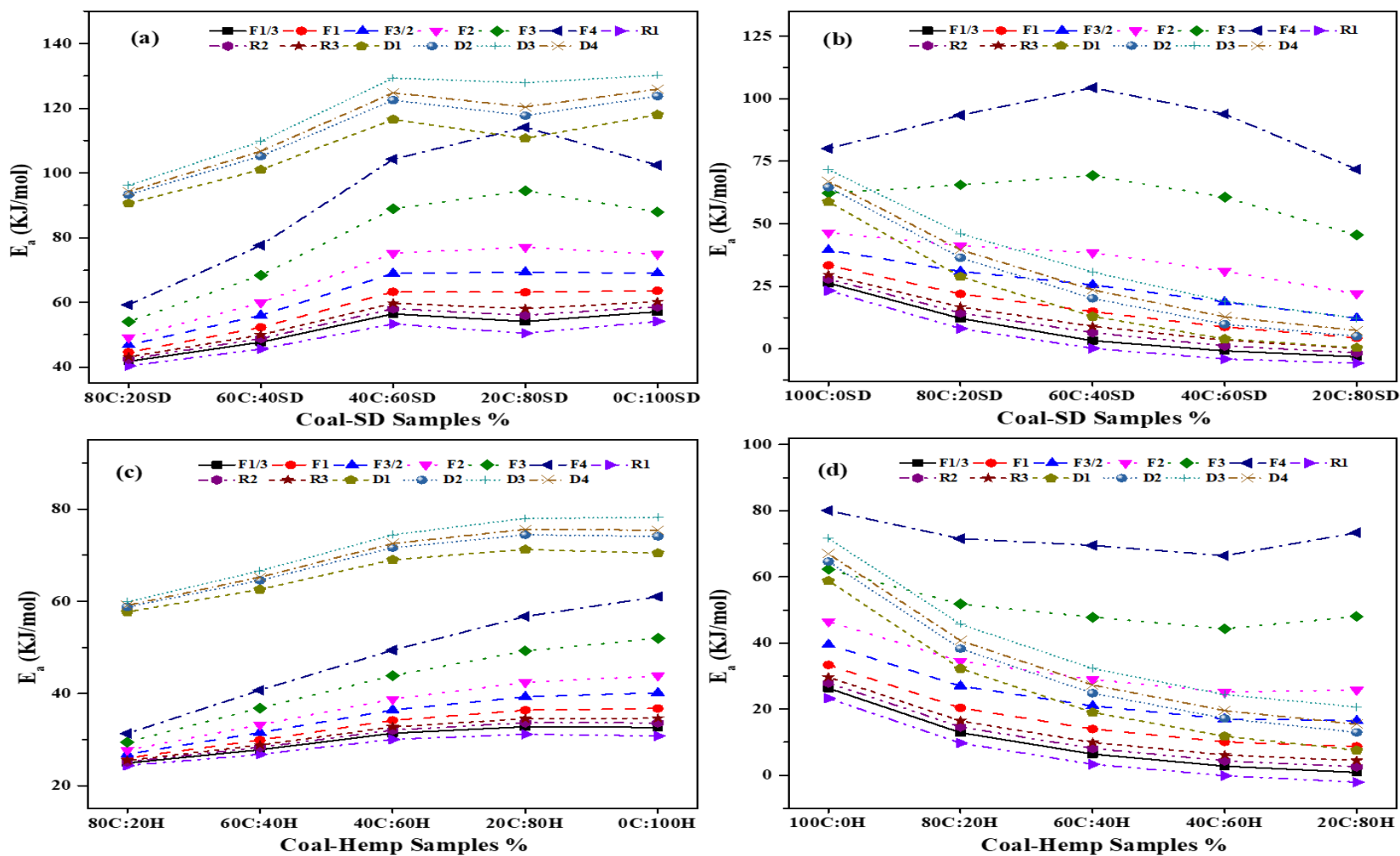


**Figure 4-4**  $E_a$  of thirteen models for coal-biomass samples (a) C-SD first stage (b) C-SD second stage (c) C-H first stage (d) C-H second stage

**Table 4-4** Co-pyrolysis kinetics parameters calculation for coal-biomass blends

<b>Sample</b>	<b>Stage</b>	<b><math>g(\alpha)</math></b>	<b>E (kJ mol<sup>-1</sup>)</b>	<b>A (min<sup>-1</sup>)</b>	<b>R<sup>2</sup></b>
100C	Second	F3/2	39	53	0.99
80C:20SD	First	R3	43	77	0.99
	Second	F3/2	31	22	0.99
60C:40SD	First	R3	49	476	0.99
	Second	F3/2	26	13	0.99
40C:60SD	First	R3	59	4832	0.99
	Second	F3/2	19	4.92	0.99
20C:80SD	First	R3	58	4290	0.99
	Second	F3/2	12	1.25	0.99
100SD	First	R3	60	6208	0.99
80C:20H	First	F2	29	15.90	1.00
	Second	F1	26	6.38	0.99
60C:40H	First	F2	33	68	0.99
	Second	F3/2	21	3.32	0.99
40C:60H	First	F2	39	351	0.99
	Second	F3/2	17	1.96	0.99
20C:80H	First	F2	42	1053	0.99
	Second	F1	9	0.24	0.99
100H	First	F2	44	1731	0.98

#### 4.4 Thermodynamics parameters

The thermodynamic parameters such as  $\Delta H$ ,  $\Delta G$ , and  $\Delta S$  were calculated by using kinetics parameters of best-fitted  $g(\alpha)$ . Table 4-5 shows the thermodynamics parameters for co-pyrolysis that were calculated from DTG peak temperature of decomposition ( $T_p$ ) for each stage. The values of  $\Delta H$  in the first stage were greater than the second stage for all coal-biomass samples. All samples show the positive value for  $\Delta H$ , which is indicating

that the pyrolysis reactions are endothermic [30]. The  $\Delta H$  followed the same pattern as  $E_a$  increased with increasing the ratio of biomass in the blend during the first stage.

**Table 4-5** Co-pyrolysis thermodynamic parameters calculation for coal-biomass blends

Sample	Stage	$\Delta H$ (kJ mol <sup>-1</sup> )	$\Delta G$ (kJ mol <sup>-1</sup> )	$\Delta S$ (kJ mol <sup>-1</sup> K <sup>-1</sup> )
100C	Second	33	201	-0.227
80C:20SD	first	38	184	-0.223
	second	25	194	-0.234
60C:40SD	first	44	181	-0.208
	second	20	191	-0.239
40C:60SD	first	54	178	-0.189
	second	13	187	-0.247
20C:80SD	first	53	175	-0.190
	second	6	182	-0.247
100SD	first	55	176	-0.187
80C:20H	first	24	169	-0.236
	second	21	201	-0.245
60C:40H	first	28	165	-0.224
	second	15	195	-0.250
40C:60H	first	34	161	-0.210
	second	11	192	-0.254
20C:80H	first	37	161	-0.201
	second	3	197	-0.272
100H	first	39	160	-0.197

The  $\Delta H$  for 100C (33kJ/mol) was less than 100SD (55 kJ/mol) and 100H (39 kJ/mol). While the difference between the value of  $\Delta H$  and  $\Delta E$  was 4-7 kJ/mol that indicates the reaction was possible to produce because it lower the potential energy barrier [31]. The value of  $\Delta H$  for C-SD blends in the first stage was 33-53 kJ/mol, whereas in the second stage was 6-25 kJ/kg. For C-H blends the  $\Delta H$  was in the range of 24-37 kJ/kg, and

for the second stage, it was 3-21 kJ/kg. The value of  $\Delta H$  for C-SD and C-H blends is depending on the value of  $E_a$ . The higher value of  $\Delta H$  for C-SD blends as compared to C-H blends was due to the complexity in chemical reaction for 100SD as compared to 100H biomass. The  $\Delta G$  specifies entire energy rises in system as the activated complexes were produced by consuming the reactants [27]. The  $\Delta G$  for 100C (201 kJ/mol) was highest as compared to 100SD (176 kJ/mol) and 100H (160 kJ/mol). The value of  $\Delta G$  was lower than 100C and 100SD which means 100H requires less energy to form an active complex [32]. The  $\Delta G$  for C-SD blends in the first stage was 175-184 kJ/kg, while for the second stage it was 182-194 kJ/kg. The range of  $\Delta G$  for C-H blends during the first stage was in the range of 161-169 kJ/mol, while in the second stage it was in the range of 197-201 kJ/mol. It could be seen that the values of  $\Delta G$  were positive for all coal-biomass blends that indicating the external energy is required to promote the reaction because the reactions are complicated [31].

The  $\Delta S$  describes the degree of disorder in the system after pyrolysis [32]. The value of  $\Delta S$  for 100C (-0.227 kJ/mol.K) was lower than 100SD (-0.187 kJ/mol.K) and 100H (-0.197 kJ/mol.K) that indicating lower the activity of 100C during pyrolysis reaction and it takes much time for chemical and physical change to move toward thermodynamic equilibrium [33]. The  $\Delta S$  was negative for all coal-biomass blends that indicates the thermodynamic equilibrium is nearer to achieve in the system [32].

## 4.5 Bio-char characterization

The yield of biochar obtained from pyrolysis of raw hemp was 40% g at 520°C that was calculated from Eq. 3-12. The produced bio-char is characterized using various techniques to investigate its suitability for various novel applications. The FTIR spectra of hemp bio-char showed a difference in functional groups and band intensities from raw hemp biomass as shown in Figure 4-5 (a). Hemp bio-char showed three major peaks of absorption. The first absorption peak at 1411  $\text{cm}^{-1}$  is attributed to benzene C-H groups for lignin [34]. The second peak was observed at 1015  $\text{cm}^{-1}$  that is mainly due to stretching vibration in C-O group. The third sharp peak at 871  $\text{cm}^{-1}$  is attributed to the aromatic C-H bending [35]. The loss of intensity at 1613  $\text{cm}^{-1}$  relative to that at 871  $\text{cm}^{-1}$  is due to the

transitional process from aliphatic structure to aromatic structure in bio-char [36]. In bio-char, hemicellulose, and cellulose functional groups were disappeared with increasing the pyrolysis temperature. Therefore, the O-H and aliphatic C-H bonds are gradually disappeared or weakened in bio-char as compared to raw hemp biomass[33], while the additional peak at  $871\text{ cm}^{-1}$  is due to the transitional process of functional groups.

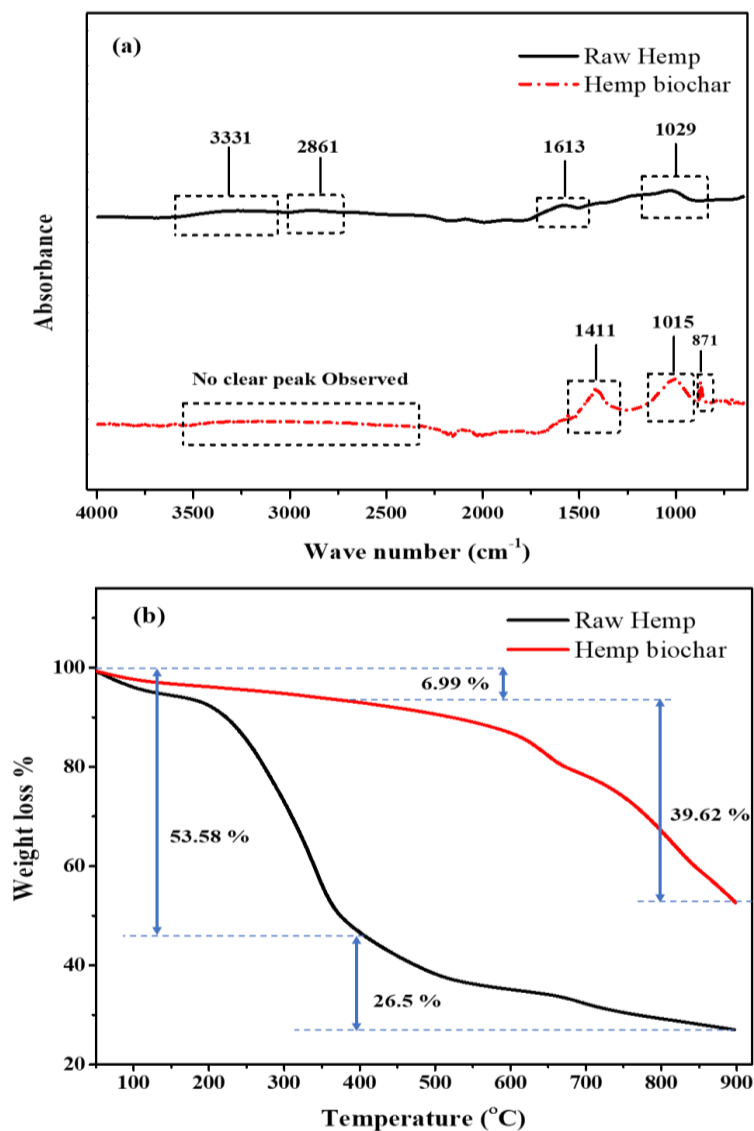


**Figure 4-5** Characterisation of raw hemp and hemp-derived bio-char (a) FTIR (b) TGA

Figure 4-5 (b) represents the TGA of raw hemp biomass and its bio-char. The overall ML of raw hemp was about 80%, while for hemp bio-char was nearly 47%. At  $400\text{ }^{\circ}\text{C}$ ,

the ML of raw hemp was 53.58%, whereas for hemp bio-char it was 6.99 % that is due to the formation temperature of hemp bio-char being 520 °C and it is thermally stable below the temperature, it was produced [37]. Additionally, the cellulose component of bio-char will be pyrolyzed above 400 °C. The ML around 400 °C temperature during pyrolysis is mainly due to the decarboxylation and the cleavage of methoxyl groups [38]. Therefore, less weight loss% in this range for bio-char indicated the elimination of these groups. The high pyrolysis temperature increases the thermal stability of biochar that makes the feasibility of biochar utilization as a fuel in co-firing with coal and other environmental applications [39].

The structural morphology of the hemp biochar and elemental scattering were analyzed by SEM coupled with EDX analysis. The SEM analysis of the hemp bio-char is shown in Figure 4-6 (a-c), while. Figure 4-6 (d) represents the EDX analysis of bio-chars. The hemp bio-char shows well defined and evenly distributed structure with horizontal and vertical tubes having uniform pores. The pores were prominent, large, and visible, it is due to the elimination of volatiles at higher pyrolysis temperature that enhances the surface area and roughness, cracks, pores, active sites and hence improving the retention and adsorption capacities of bio-char [40]. The SEM analysis of the hemp bio-char shows that it has the potential to be utilized in multiple applications such as catalysis and environmental applications. The EDX analysis revealed the existence of important elements in hemp bio-char such as Mg, Ca, K, Si, O, and C. These all are essential elements to enhance soil fertility as well as define the potential of hemp bio-char in agricultural applications. Detailed studies to further investigate the particular influence of hemp bio-char for agricultural applications are still needed.

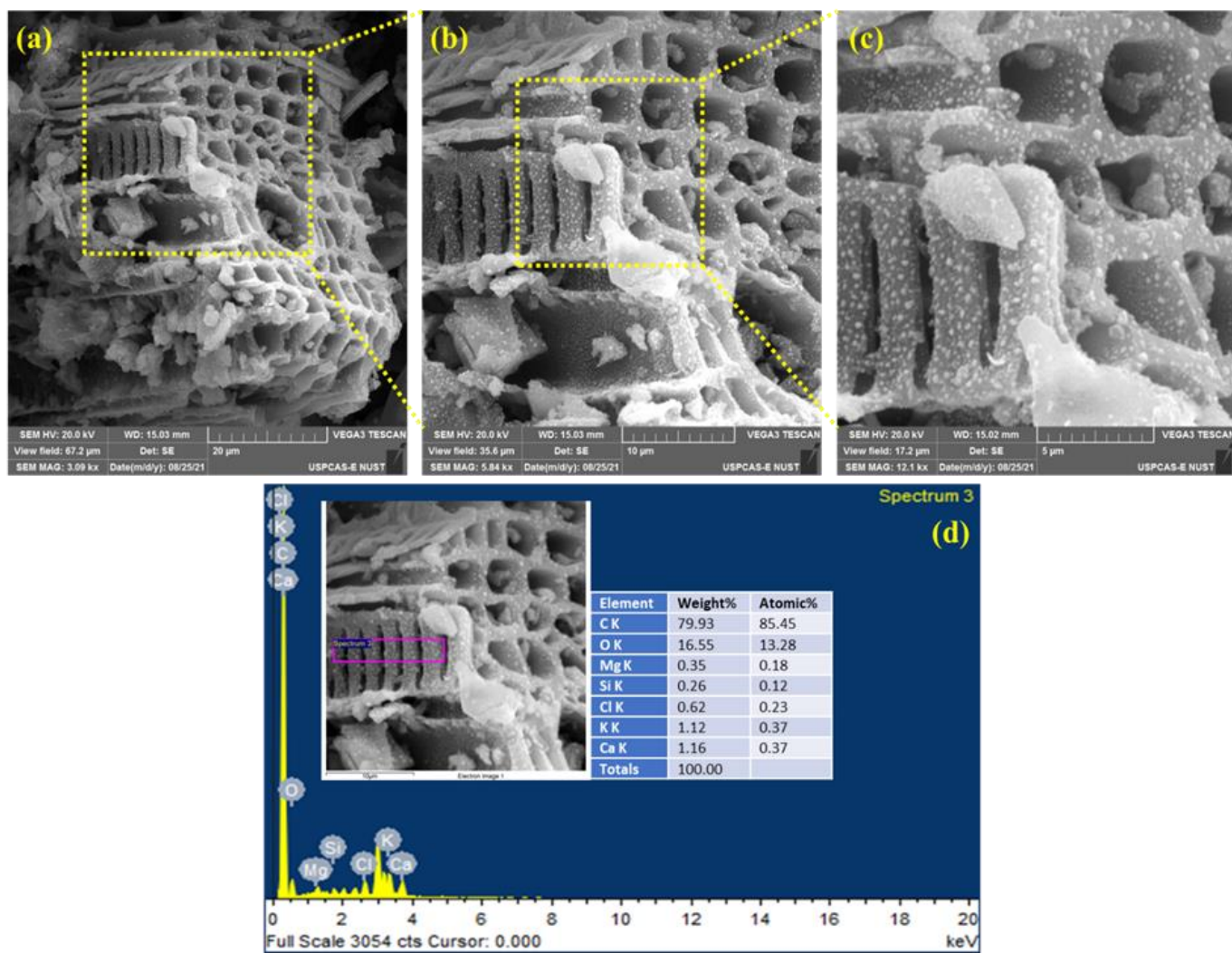


**Figure 4-6** Hemp-derived bio-char (a-c) SEM analysis (d) EDX elemental analysis

## Summary

The coal-biomass blends were characterized by CHN, GCV, FTIR, and TGA. The CHN analysis investigates that the carbon content of coal-biomass blends increases as the ratio of coal in the blend is increased. While the hydrogen content of both biomasses was higher than 100C. The higher content of hydrogen in biomass act as a hydrogen donor in the pyrolysis of coal. The nitrogen content of 100C is slightly higher than 100SD but less than 100H. Therefore, C-SD blends aid in reducing NO<sub>x</sub> emissions. The GCV analysis showed that the 100C has the highest GCV (29.6 MJ/kg) as compared to 100SD (20.5 MJ/kg) and 100H (18 MJ/kg). When coal is blended with biomass, it increases the GCV of coal-biomass blends due to an increase in carbon content percentage. It means that the obtained products from co-pyrolysis also have a high calorific value as compared to only biomass pyrolysis products.

The FTIR analysis reveals that the functional groups in coal and biomass were quite same but the absorption intensities were different. The 100C was rich in aromatic C=C, while both biomasses mostly contain O-H groups. For coal-biomass blends, the band intensity of O-H stretching is reduced and the intensity of aromatic ring C=C increases. This situation may be due to the reduction of oxygen and hydrogen content from biomass by blending it with coal that further increases the carbon content of coal-biomass blends. Co pyrolysis was performed in TGA and the analysis investigate that ML was in the following order 100SD>100H>100C. Whereas, the RL was in reverse order. The coal-biomass blends showed some similar properties to those of individual fuels. It is observed the ML, RL,  $(dw/dt)_{max}$ ,  $T_i$ , and  $T_p$  of coal-biomass blends vary with increasing or decreasing blending ratio of biomass. The TGA results show that C-SD blends are suitable to produce bio-oil, while the C-H blends are suitable for the production of bio-char.

The synergistic effect is mostly present in C-H blends rather than C-SD blends in terms of ML. From C-SD blends the 20C:80SD shows somehow positive synergy, while for C-H blends the 80C:20H, 60C:40H, and 40C:60H show a positive synergistic effect in terms of ML. The kinetic parameters demonstrate that the  $E_a$  was in the following order 100C<100H<100SD. The  $E_a$  for 100C was 39 kJ mol<sup>-1</sup> through F3/2, while 100SD and

100H showed  $60 \text{ kJ mol}^{-1}$  through R3 and  $44 \text{ kJ mol}^{-1}$  through the F2 model, respectively. The  $E_a$  for coal-biomass blend in the first stage increased as the ratio of biomass increased, whereas in the second stage the  $E_a$  decreased as the percentage of biomass increased in coal-biomass blends.

Thermodynamic parameters show that all coal-biomass blends have a positive value for  $\Delta H$ , which is indicating that the pyrolysis reactions are endothermic. The values of  $\Delta G$  were positive for all coal-biomass blends that indicating external energy is required to promote the reaction because the reactions are complicated. The value of  $\Delta S$  showed the negative value for all coal-biomass blends that indicating the system is close to its thermodynamic equilibrium. The FTIR, TGA, and SEM-EDX of hemp bio-char show that it can be used in energy and agriculture applications.

## References

1. Demirbas, A., *Combustion characteristics of different biomass fuels*. Progress in Energy and Combustion Science, 2004. **30**(2): p. 219-230.
2. Gaqa, S., et al., *The Properties and Suitability of Various Biomass/Coal Blends for Co-Gasification Purposes*. Journal of Sustainable Bioenergy Systems, 2014. **04**: p. 175-182.
3. Vassilev, S.V., C.G. Vassileva, and V.S. Vassilev, *Advantages and disadvantages of composition and properties of biomass in comparison with coal: An overview*. Fuel, 2015. **158**: p. 330-350.
4. Obernberger, I. and G. Thek, *Physical characterisation and chemical composition of densified biomass fuels with regard to their combustion behaviour*. Biomass and Bioenergy, 2004. **27**(6): p. 653-669.
5. Dhar, S.A., T.U. Sakib, and L.N. Hilary, *Effects of pyrolysis temperature on production and physicochemical characterization of biochar derived from coconut fiber biomass through slow pyrolysis process*. Biomass Conversion and Biorefinery, 2020.
6. Zhang, C., et al., *Co-pyrolysis characteristics of camellia oleifera shell and coal in a TGA and a fixed-bed reactor*. Journal of Analytical and Applied Pyrolysis, 2021. **155**: p. 105035.
7. Kraszkiewicz, A., et al., *Assessment of the Possibility of Using Hemp Biomass (Cannabis Sativa L.) for Energy Purposes: A Case Study*. Applied Sciences, 2019. **9**(20).
8. Jenkins, B., *Physical properties of biomass*. Biomass handbook, 1989: p. 860-891.
9. Chen, X., et al., *Pyrolysis characteristics and kinetics of coal–biomass blends during co-pyrolysis*. Energy & Fuels, 2019. **33**(2): p. 1267-1278.
10. Zhou, Y., et al., *Surface hydrophobicity of sub-bituminous and meta-bituminous coal and their flotation kinetics*. Fuel, 2019. **242**: p. 416-424.
11. Chen, S., et al., *Effect of oxidation processing on the surface properties and floatability of Meizhiyou long-flame coal*. Fuel, 2017. **210**: p. 177-186.
12. Dai, L., et al., *Hydrothermal pretreatment of bamboo sawdust using microwave irradiation*. Bioresource Technology, 2018. **247**: p. 234-241.
13. Rajinipriya, M., et al., *Single stage purification of flax, hemp, and milkweed stem and their physical and morphological properties*. International Journal of Polymer Analysis Characterization, 2018. **23**(1): p. 78-88.
14. Moonart, U. and S. Utara, *Effect of surface treatments and filler loading on the properties of hemp fiber/natural rubber composites*. Cellulose, 2019. **26**(12): p. 7271-7295.
15. Zhao, J., et al., *Effects of post-washing on pretreated biomass and hydrolysis of the mixture of acetic acid and sodium hydroxide pretreated biomass and their mixed filtrate*. Bioresource Technology, 2021: p. 125605.
16. Mallick, D., et al., *Discernment of synergism in pyrolysis of biomass blends using thermogravimetric analysis*. Bioresource Technology, 2018. **261**: p. 294-305.
17. Anca-Couce, A., A. Berger, and N. Zobel, *How to determine consistent biomass pyrolysis kinetics in a parallel reaction scheme*. Fuel, 2014. **123**: p. 230-240.

18. Sadhukhan, A.K., et al., *Modelling of pyrolysis of coal–biomass blends using thermogravimetric analysis*. *Bioresource Technology*, 2008. **99**(17): p. 8022-8026.
19. Chen, X., et al., *Thermogravimetric analysis and kinetics of the co-pyrolysis of coal blends with corn stalks*. *Thermochimica Acta*, 2018. **659**: p. 59-65.
20. Laougé, Z.B. and H. Merdun, *Investigation of thermal behavior of pine sawdust and coal during co-pyrolysis and co-combustion*. *Energy*, 2021. **231**: p. 120895.
21. Ulloa, C.A., A.L. Gordon, and X.A. García, *Thermogravimetric study of interactions in the pyrolysis of blends of coal with radiata pine sawdust*. *Fuel Processing Technology*, 2009. **90**(4): p. 583-590.
22. Merdun, H. and Z.B. Laougé, *Kinetic and thermodynamic analyses during co-pyrolysis of greenhouse wastes and coal by TGA*. *Renewable Energy*, 2021. **163**: p. 453-464.
23. Guo, F., et al., *Characterization of Zhundong lignite and biomass co-pyrolysis in a thermogravimetric analyzer and a fixed bed reactor*. *Energy*, 2017. **141**: p. 2154-2163.
24. Özsin, G. and A.E. Pütün, *Co-pyrolytic behaviors of biomass and polystyrene: Kinetics, thermodynamics and evolved gas analysis*. *Korean Journal of Chemical Engineering*, 2018. **35**(2): p. 428-437.
25. Toptas, A., et al., *Combustion behavior of different kinds of torrefied biomass and their blends with lignite*. *Bioresource Technology*, 2015. **177**: p. 328-336.
26. Tian, H., et al., *Co-pyrolysis of Miscanthus Sacchariflorus and coals: A systematic study on the synergies in thermal decomposition, kinetics and vapour phase products*. *Fuel*, 2020. **262**: p. 116603.
27. Naqvi, S.R., et al., *Synergistic effect on co-pyrolysis of rice husk and sewage sludge by thermal behavior, kinetics, thermodynamic parameters and artificial neural network*. *Waste Management*, 2019. **85**: p. 131-140.
28. Balasundram, V., et al., *Thermogravimetric catalytic pyrolysis and kinetic studies of coconut copra and rice husk for possible maximum production of pyrolysis oil*. *Journal of Cleaner Production*, 2017. **167**: p. 218-228.
29. Chong, C.T., et al., *Pyrolysis characteristics and kinetic studies of horse manure using thermogravimetric analysis*. *Energy Conversion and Management*, 2019. **180**: p. 1260-1267.
30. Huang, L., et al., *Thermodynamics and kinetics parameters of co-combustion between sewage sludge and water hyacinth in CO<sub>2</sub>/O<sub>2</sub> atmosphere as biomass to solid biofuel*. *Bioresource Technology*, 2016. **218**: p. 631-642.
31. Ming, X., et al., *Thermal degradation of food waste by TG-FTIR and Py-GC/MS: Pyrolysis behaviors, products, kinetic and thermodynamic analysis*. *Journal of Cleaner Production*, 2020. **244**: p. 118713.
32. Ni, Z., et al., *Research on the co-pyrolysis of coal gangue and coffee industry residue based on machine language: Interaction, kinetics, and thermodynamics*. *Science of The Total Environment*, 2022. **804**: p. 150217.
33. Xu, Y. and B. Chen, *Investigation of thermodynamic parameters in the pyrolysis conversion of biomass and manure to biochars using thermogravimetric analysis*. *Bioresource Technology*, 2013. **146**: p. 485-493.

34. Kim, D., K. Lee, and K.Y. Park, *Upgrading the characteristics of biochar from cellulose, lignin, and xylan for solid biofuel production from biomass by hydrothermal carbonization*. *Journal of Industrial and Engineering Chemistry*, 2016. **42**: p. 95-100.
35. Zhang, C., et al., *Characterization of biochars derived from different materials and their effects on microbial dechlorination of pentachlorophenol in a consortium*. *RSC Advances*, 2019. **9**(2): p. 917-923.
36. Keiluweit, M., et al., *Dynamic molecular structure of plant biomass-derived black carbon (biochar)*. *Environmental Science & Technology* 2010. **44**(4): p. 1247-1253.
37. Zhao, S.-X., N. Ta, and X.-D. Wang, *Effect of Temperature on the Structural and Physicochemical Properties of Biochar with Apple Tree Branches as Feedstock Material*. *Energies*, 2017. **10**(9).
38. Hu, J., et al., *Effect of temperature on structure evolution in char from hydrothermal degradation of lignin*. *Journal of Analytical and Applied Pyrolysis*, 2014. **106**: p. 118-124.
39. Parvez, A.M., J.D. Lewis, and M.T. Afzal, *Potential of industrial hemp (Cannabis sativa L.) for bioenergy production in Canada: Status, challenges and outlook*. *Renewable and Sustainable Energy Reviews*, 2021. **141**: p. 110784.
40. Ahmed, A., et al., *Sawdust pyrolysis from the furniture industry in an auger pyrolysis reactor system for biochar and bio-oil production*. *Energy Conversion and Management*, 2020. **226**: p. 113502.

# Chapter 5

## Conclusions and Recommendations

### 5.1 Conclusions

The coal-biomass blends were prepared with different blending ratios for co-pyrolysis. The CHN and GCV analysis results indicated that 100C has higher carbon content and gross calorific value as compared to 100SD and 100H biomass, while the coal-biomass blends showed intermediate behaviour those of individual fuels. FTIR analysis showed that both biomasses have nearly the same functional groups while having different absorbance intensities. Thermal decomposition characteristics of coal-biomass blends were investigated by TGA. The decomposition of biomass occurred in three main stages such as moisture release, cellulose and hemicellulose degradation, and lignin decomposition. The  $T_i$  and  $T_p$  of the reaction were influenced by the blending ratio. The deviation between the experimental and calculated values of ML, RL, and  $DTG_{max}$  showed the positive or negative values that indicate the presence of a synergistic effect or inhibitory effect, respectively. Kinetics parameters ( $E_a$  and  $A$ ) were calculated by the Coats-Redfern method with thirteen integral functions. The  $E_a$  for 100C was  $39 \text{ kJ mol}^{-1}$ , for 100SD was  $60 \text{ kJ mol}^{-1}$  and for 100H was  $44 \text{ kJ mol}^{-1}$ . The  $E_a$  of blends in the first stage increased as the ratio of biomass increased in the blends, while in the second stage the  $E_a$  decreased as the ratio of biomass increased in blends. Thermodynamic parameters showed that  $\Delta H$  and  $\Delta G$  were positive values for each coal-biomass blend which means reaction was endothermic and non-spontaneous, Also, the  $\Delta S$  was negative for each coal-biomass blend that indicates the more ordered state or the system is close to its thermodynamic equilibrium. As the C-SD blends produced more volatiles during co-pyrolysis, it could be a strong candidate to produce bio-oil, while the C-H blends were suitable to produce biochar as they left more residue after co-pyrolysis. Hemp biochar has the potential to be utilized in adsorption, carbon sequestration, and heat and power generation applications.

## 5.2 Recommendations

Co pyrolysis of coal-biomass is an efficient and partially greener way to produce liquid, gaseous, and solid fuels. But the major challenge that resists its large-scale application is designing of co-pyrolysis reactor because coal and biomass both have different kinetic and thermodynamic behavior. Therefore, the reactor design can be performed in future by considering experimental results.

The synergistic effect can be observed through CHN, GCV, and FTIT. Additionally, model free kinetics at different heating rate can be performed to better understand the comparison in model free and model fitting methods.

Furthermore, hemp bio-char has the potential to be utilized in catalytic, agriculture, and energy production application, therefore it needs more exploration through characterizations for their applicability.

# Appendix A

**“Investigating the characterisation, kinetic mechanism, and thermodynamic behaviour of coal-biomass blends in co-pyrolysis process”. Hamad Gohar<sup>1</sup>, Asif Hussain Khoja\*, Abeera Ayaz Ansari, Rabia Liaquat, Salman Raza Naqvi, Muhammad Hassan, Khalil Hasni, Umair Yaqub Qazi and Imtiaz Ali.**

Process Safety and Environmental Protection. (Under review)

The screenshot displays the Editorial Manager interface for the journal "Process Safety and Environmental Protection". The user is logged in as "Hamad Gohar" with the role of "Author". The page title is "Submissions Being Processed for Author". The submission details are as follows:

Action	Manuscript Number	Title	Authorship	Initial Date Submitted	Status Date	Current Status
<a href="#">Action Links</a>	PSEP-D-22-00024	Investigating the characterization, kinetic mechanism, and thermodynamic behaviour of coal-biomass blends in co-pyrolysis process	Other Author	Jan 07, 2022	Feb 12, 2022	Under Review